



1 **Single-particle characterization of aerosols collected at a remote site in the Amazonian**  
2 **rainforest and an urban site in Manaus, Brazil**

3

4 Li Wu<sup>1</sup>, Xue Li<sup>1</sup>, HyeKyeong Kim<sup>1</sup>, Hong Geng<sup>2</sup>, Ricardo H. M. Godoi<sup>3</sup>, Cybelli G. G. Barbosa<sup>3</sup>,  
5 Ana F. L. Godoi<sup>3</sup>, Carlos I. Yamamoto<sup>4</sup>, Rodrigo A. F. de Souza<sup>5</sup>, Christopher Pöhlker<sup>6</sup>, Meinrat  
6 O. Andreae<sup>6,7</sup>, and Chul-Un Ro<sup>1,\*</sup>

7

8 <sup>1</sup>Department of Chemistry, Inha University, Incheon, 402-751, Korea;

9 <sup>2</sup>Institute of Environmental Science, Shanxi University, Taiyuan 030006, China;

10 <sup>3</sup>Environmental Engineering Department, Federal University of Parana-UFPR, Curitiba, PR,  
11 Brazil;

12 <sup>4</sup>Chemical Engineering Department, Federal University of Paraná-UFPR, Curitiba, PR, Brazil;

13 <sup>5</sup>Amazonas State University, Superior School of Technology, Manaus, Amazonas, Brazil;

14 <sup>6</sup>Multiphase Chemistry & Biogeochemistry Departments, Max Planck Institute for Chemistry,  
15 55020 Mainz, Germany;

16 <sup>7</sup>Department of Geology and Geophysics, King Saud University, Riyadh, Saudi Arabia.

17

18 **Abstract**

19 In this study, aerosol samples collected at a remote site in the Amazonian rainforest and an urban  
20 site in Manaus, Brazil, were investigated on a single particle basis using a quantitative energy-  
21 dispersive electron probe X-ray microanalysis (ED-EPMA). Twenty-three aerosol samples were  
22 collected in four size ranges (0.25-0.5, 0.5-1.0, 1.0-2.0, and 2.0-4.0  $\mu\text{m}$ ) during the wet season in  
23 2012 at two Amazon basin sites: 10 samples in Manaus, an urban area; and 13 samples at an 80-m  
24 high tower, located at the Amazon Tall Tower Observatory (ATTO) site in the middle of the  
25 rainforest, 150 km northeast of Manaus. The aerosol particles were classified into nine particle

---

\*Corresponding author. Tel.: +82 32 860 7676; fax: +82 32 874 9207

E-mail address: [curo@inha.ac.kr](mailto:curo@inha.ac.kr) (C.-U. Ro)



26 types based on the morphology on the secondary electron images (SEIs) together with the  
27 elemental concentrations of 3,162 individual particles: (i) secondary organic aerosols (SOA), (ii)  
28 ammonium sulfate (AS), (iii) SOA and AS mixtures, (iv) aged mineral dust, (v) reacted sea-salts,  
29 (vi) primary biological aerosol (PBA), (vii) carbon-rich or elemental carbon (EC) particles, such  
30 as soot, tar ball, and char, (viii) fly ash, and (ix) heavy metal (HM, such as Fe, Zn, Ni, and Ti)-  
31 containing particles. In submicron aerosols collected at the ATTO site, SOA and AS mixture  
32 particles were predominant (50-94% in relative abundance) with SOA and ammonium sulfate  
33 comprising 73-100%. In supermicron aerosols at the ATTO site, aged mineral dust and sea-salts  
34 (37-70%) as well as SOA and ammonium sulfate (28-58%) were abundant. PBAs were observed  
35 abundantly in the  $PM_{2.4}$  fraction (46%), and EC and fly ash particles were absent in all size  
36 fractions. The analysis of a bulk  $PM_{0.25-0.5}$  aerosol sample from the ATTO site using Raman  
37 microspectrometry and attenuated total reflection Fourier transform infrared spectroscopy showed  
38 that ammonium sulfate, organics, and minerals are the major chemical species, which is consistent  
39 with the ED-EPMA results. In the submicron aerosols collected in Manaus, either SOA and  
40 ammonium sulfate (17-80%) or EC particles (6-78%) were dominant depending on the samples.  
41 In contrast, aged mineral dust, reacted sea-salt, PBA, SOA, ammonium sulfate, and EC particles  
42 comprised most of the supermicron aerosols collected in Manaus. The SOA, ammonium sulfate,  
43 and PBAs were mostly of a biogenic origin from the rainforest, whereas the EC and HM-containing  
44 particles were of an anthropogenic origin. Aged mineral dust and reacted sea-salt particles,  
45 including mineral dust mixed with sea-salts probably during long-range transatlantic transport,  
46 were abundant in the supermicron fractions at both sites. Among the aged mineral dust and reacted  
47 sea-salt particles, sulfate-containing ones outnumbered those containing nitrates and  
48 sulfate+nitrate in the ATTO samples. In contrast, particles containing sulfate+nitrate were  
49 comparable in number to particles containing sulfate only in the Manaus samples, indicating the  
50 different sources and formation mechanisms of secondary aerosols, i.e., the predominant presence  
51 of sulfate at the ATTO site from mostly biogenic emissions and the elevated influences of nitrates  
52 from anthropogenic activities at the Manaus site.

53

## 54 1. Introduction

55 The Amazonian rainforest is regarded as one of the primitive continental regions and  
56 atmospheric aerosol particles over the region are expected to be influenced minimally by



57 anthropogenic activities, particularly during the wet season (Andreae, 2007; Martin et al., 2010b;  
58 Chen et al., 2015). The unique near-natural conditions during the wet season make it an ideal place  
59 to understand the occurrence, nature, origin, and transport of aerosol particles, which can directly  
60 scatter and absorb solar radiation and indirectly serve as cloud condensation nuclei (CCN) and/or  
61 ice nuclei (IN), to better predict the additional anthropogenic effects on aerosol particles, and to  
62 help determine their influences on the environment, climate, and human health (Artaxo et al.,  
63 2013).

64 Many studies have been performed on the aerosol characteristics in the Amazon basin, but  
65 the formation and interaction of airborne Amazonian aerosols are not completely understood  
66 (Andreae et al., 2015; Martin et al., 2010a, 2016; Fraund et al., 2017; Fan et al., 2018). The Amazon  
67 Basin atmosphere is near-pristine during the wet season, whereas biomass burning prevails during  
68 the dry season (Andreae et al., 2007; Pöschl et al., 2010; Artaxo et al., 2013; Pöhlker et al., 2018).  
69 Based on a long-term study, it was reported that aerosol particles in the coarse fraction are  
70 relatively constant in concentrations through the wet and dry seasons, whereas the aerosol particle  
71 levels in the fine fraction differ due to the predominant influence of biomass burning during the  
72 dry season (Artaxo et al., 2013; Moran-Zuloaga et al., 2018). Scanning electron microscopy/energy  
73 dispersive X-ray spectrometry (SEM/EDX) studies categorized the Amazonian aerosols mainly as  
74 secondary organic aerosol (SOA) particles, sulfates/chlorides, primary biological aerosol (PBA)  
75 particles, mineral dust, sea salts (fresh and/or aged), and pyrogenic carbon particles within the  
76 different size fractions (Krejci et al., 2005; Pöschl et al., 2010). Over the Amazonian rainforest,  
77 SOA particles are formed through the condensation of biogenic organic compounds onto biogenic  
78 K-rich salt particles emitted from the forest and are predominant in the fine fraction, which are  
79 important for CCN (Pöhlker et al., 2012) and can also affect the potential of mineral particles when  
80 acting as an organic coating (Möhler et al., 2008). Under high relative humidity conditions, nano-  
81 and micrometer SOA particles with a dominance of  $\alpha$ -pinene and isoprene as their precursors can  
82 remain in the liquid phase (Bateman et al., 2016), which further enhances the formation of SOA  
83 as well as the oxygen-to-carbon (O/C) ratios. Hence, the study of this particle type can help  
84 elucidate some of the atmospheric interactions (Lin et al., 2014). In addition, the hygroscopicity  
85 of complex ambient organic particles from the Amazon Basin was well simulated by a mixture of  
86 organic surrogates consisting of levoglucosan, 4-hydroxybenzoic acid, and humic acid (Lei et al.,  
87 2018). The atmosphere in the Amazon Basin is also rich in PBA particles (Andreae, 2007; Artaxo



88 et al., 1998, 2013; Martin et al., 2010a). Their unique morphology and elemental compositions of  
89 major C and O with minor S, K, P, Na, N, Cl, and/or Mg obtained by SEM/EDX are characteristic  
90 of individual PBAs like fungal spores (China et al., 2016). PBA particles can contribute to CCN  
91 after being transported to cloud formation altitudes by strong convection (Artaxo et al., 2013).

92 The Amazon Tall Tower Observatory (ATTO) consists of several observatory towers built  
93 in the middle of the Amazon rainforest for a continuous and detailed study of biota-atmosphere  
94 interactions (Andreae et al., 2015). At the ATTO site, single particle analysis by a combination of  
95 scanning transmission X-ray microscopy/near edge X-ray absorption fine structure spectroscopy  
96 (STXM/NEXAFS) and SEM/EDX highlighted the dominance of biological particles (Fraund et  
97 al., 2017). Very few cluster varieties were observed without anthropogenic elements that were  
98 found near a capital city, Manaus. The abundance of biogenic SOA and the presence of C, N, O, P  
99 and K are characteristic of aerosols at the area (Fraund et al., 2017).

100 Manaus, the capital of Amazonas state, is a large city located in the northern region of  
101 Brazil with more than 2 million inhabitants in an area of 11,401 km<sup>2</sup> (IBGE, 2017). The city, which  
102 is surrounded by the largest tropical rainforest, has a large industrial zone, a port area at the Rio  
103 Negro, an energy matrix based on fuel oil, diesel, and natural gas, and a growing automotive fleet  
104 (Martin et al, 2010a, 2016). Consequently, the pollution plume from Manaus can act as a laboratory  
105 for examining the perturbations in natural processes (Martin et al, 2016). Based on an investigation  
106 on particulate matter during the wet season, more oxidized organic components were observed to  
107 be present at sites downwind of Manaus than the upwind ones (de Sá et al., 2018), of which one  
108 third was of an urban origin (Palm et al., 2018).

109 Only a few studies examined airborne particles over the Amazon rainforest and nearby  
110 urban sites simultaneously (Fraund et al., 2017; Martin et al., 2016). Therefore, there is still little  
111 information on the urban vs. ecosystem influences. In this study, twenty-three aerosol samples  
112 collected at the ATTO site and at an urban site in Manaus during the wet season in 2012 were  
113 examined on a single particle basis using a quantitative energy-dispersive electron probe X-ray  
114 microanalysis (ED-EPMA), which provided information on the morphology and chemical  
115 compositions of aerosols containing both light and heavy elements. This paper presents the  
116 different characteristics of the aerosols collected at the rainforest and in Manaus.

117

## 118 2. Experimental section



## 119 2.1. Samples

120 During the wet season in 2012, aerosol samples were collected at two sampling sites on the  
121 Amazon basin, i.e., ATTO and a central area of Manaus. The ATTO site (S 02° 08.647' W 58°  
122 59.992') is situated in the Uatumã Sustainable Development Reserve, approximately 150 km  
123 northeast of Manaus (Fig. 1). This is a multidisciplinary research site of an international joint  
124 project between Brazil and Germany for continuous monitoring of the biological, physical, and  
125 chemical functions of the Amazon rainforest to answer questions related to climate change  
126 (Andreae et al., 2015). Aerosol sampling was performed at an 80-m-height walk-up tower at the  
127 ATTO site. In Manaus, the sampling site is situated in the central part of the city (S 03° 05.753',  
128 W 59° 59.419'), a representative urban site influenced mostly by vehicle traffic. Particles were  
129 collected at a 2 m height above ground level. The aerosol samples were collected on TEM grids  
130 (Ted Pella Inc., USA, Ted Pella Inc., Carbon/Formvar 200 mesh Cu grid, 35–70 nm thickness)  
131 using a five stage Battelle impactor (the cut-off diameters are 0.25, 0.5, 1, 2, and 4  $\mu\text{m}$  for stages  
132 1-5, respectively) at the ATTO and Manaus sites on April 1, 16, 17, and 18 and May 1, 2, and 3  
133 (the four- and three-day samples were collected at the ATTO and Manaus sites, which are notated  
134 as samples SA1-SA4 and SM1-SM3, respectively). On each date, the sampling started around  
135 noon (local time) and lasted for approximately 100 min. The individual particles collected on  
136 stages 1-3 (PM<sub>0.25-0.5</sub>, PM<sub>0.5-1.0</sub>, and PM<sub>1.0-2.0</sub>) for each sample and on an additional stage 4 (PM<sub>2.0-</sub>  
137 4.0) for the SA4 and SM3 samples were examined.

138 During the sampling period, the temperature was in the range of 22 to 32°C and the relative  
139 humidity was above 55%. On April 16 and May 1 and 2, rain events occurred within the previous  
140 24 hours prior to sampling. The ten-day backward air-mass trajectories were obtained using the  
141 Hybrid Lagrangian Single-Particle Integrated Trajectory (HYSPLIT) model from the NOAA Air  
142 Resources Laboratory's web server (<http://www.arl.noaa.gov/ready/hysplit4.html>), as shown in  
143 Fig. 2. All samples were influenced by transatlantic air masses at a 1000 m receptor height and the  
144 Manaus site was influenced mainly by the surrounding rainforest at 500 m and 100 m heights.

145

## 146 2.2. EPMA measurements and data analysis

147 Low-Z particle EPMA was carried out by SEM (JSM-6390, JEOL) equipped with an  
148 Oxford Link SATW ultrathin window EDX detector, which has a spectral resolution of 133 eV for  
149 Mn K $\alpha$  X-rays. The X-ray spectra were recorded using INCA Energy software. To achieve the



150 optimal experimental conditions, such as the low background level in the X-ray spectra and good  
151 sensitivity for low-*Z* element analysis, an accelerating voltage of 10 kV, a beam current of 0.5 nA,  
152 and a measuring time of 20 s were used. X-ray spectral data acquisition for individual particles  
153 was carried out manually in point analysis mode, i.e., the electron beam was focused at the center  
154 of each particle, and X-rays were acquired while the beam remained fixed on this single spot. The  
155 secondary electron images (SEIs) and X-ray spectra of an overall 3,162 individual particles for the  
156 ATTO and Manaus samples were examined. As the TEM grids are thin (35-70 nm thickness),  
157 strong X-rays from the Al or Cu metal stub commonly used in the SEM/EDX measurement would  
158 be a problem when the TEM grid substrate is placed on it. A home-made sample holder (Fig. 3(a))  
159 for the TEM grid samples was used to avoid interference from the metal stub, resulting in X-ray  
160 spectra of bare TEM grids, which showed only C and O X-ray peaks from their carbon/Formvar  
161 thin-film, a Cu-L peak caused by lateral scattering from the Cu bars of TEM grids, and a Si peak  
162 from an impurity, as shown in Fig. 3(b). The net X-ray intensities for the chemical elements were  
163 obtained by non-linear, least-square fitting of the spectra using the AXIL program (Vekemans et  
164 al., 1994). Although the characteristic X-ray intensities of C and O were low for the bare TEM  
165 grids, determination of the C and O concentrations for individual particles on the TEM grids was  
166 performed using a methodology based on the Monte Carlo calculation technique to correct for the  
167 interfering X-ray peaks of C and O emitted from the TEM grid, which provided reliable  
168 quantification results when applied to the quantification of standard (sub)micron particles, such as  
169 CaCO<sub>3</sub>, CaSO<sub>4</sub>, Na<sub>2</sub>SO<sub>4</sub>, and SiO<sub>2</sub>. On the other hand, electron beam-sensitive particles, such as  
170 NaNO<sub>3</sub>, Ca(NO<sub>3</sub>)<sub>2</sub>·4H<sub>2</sub>O, and ammonium sulfate, provided deviating quantification results (Geng  
171 et al, 2010). As the Cu-L and Si X-ray intensities from the bare TEM grids are quite small (< 20  
172 cps) under these measurement conditions, the two peaks could be neglected safely during the  
173 quantification procedure.

174

### 175 **3. Results and discussion**

#### 176 **3.1. Particle types observed in samples collected at the ATTO and Manaus sites**

177 In this study, the analyzed particles were classified based on their X-ray spectral and SEI  
178 data, where 9 different particle types were observed in the samples collected at the ATTO and  
179 Manaus sites during the wet season in 2012; i.e., (i) SOA, (ii) ammonium sulfate (AS) particles,  
180 (iii) SOA and AS mixture particles, (iv) aged (reacted) sea-salt, (v) aged mineral dust, (vi) PBA



181 particles, (vii) carbon-rich or elemental carbon (EC) particles such as soot, tar ball, and char or  
182 coal dust, (viii) fly ash particles, and (ix) heavy metal-containing (HM) particles. Based on single  
183 particle analysis for aerosol samples collected at a remote site north of Manaus, Brazil during the  
184 2008 wet season (3-13 March) using SEM/EDX, five types of aerosols, such as (i) SOA droplets,  
185 (ii) SOA-inorganic mixture particles where the inorganics are mostly sulfates and/or chlorides, (iii)  
186 PBA, (iv) mineral dust, and (v) pyrogenic carbon particles, were reported. The pure SOA droplets  
187 dominated in the nucleation and Aitken modes, whereas the pure SOA, SOA-inorganic mixture  
188 particles, and pyrogenic carbon particles dominated in accumulation mode (Pöschl, et al., 2010).  
189 With the exception of the reacted sea-salt particles probably from the Atlantic Ocean, the particle  
190 types observed in this study are comparable to their study. Figs. 4 and 5 present typical field SEIs  
191 for submicron and supermicron aerosol particles collected at the ATTO and Manaus sites,  
192 respectively, where the chemical species comprising each particle is indicated. Ammonium sulfate  
193 and SOA particles are dominant in the sub- and super-micron aerosol fractions collected at the  
194 ATTO site with some mineral particles and aged sea-salts in the supermicron fractions, whereas  
195 the aerosol samples collected at the Manaus site are composed of various types of particles of  
196 anthropogenic and/or natural origin. Figs. S1-S7 of Supporting Information present typical SEIs  
197 for all the samples with identified chemical species on the SEIs, which helps briefly illustrate the  
198 different features of the samples collected at the ATTO and Manaus sites. The characteristics of  
199 the particle types observed in the ATTO and Manaus samples are described in the following.

200

### 201 **3.1.1. Secondary organic aerosol (SOA) particles**

202 In this study, SOA particles were observed frequently in both the ATTO and Manaus  
203 samples, even though pure SOA particles were rare and most of them were mixed internally with  
204 other species, such as ammonium sulfate, K-rich salt, reacted sea-salts, etc. The SOA particles over  
205 the Amazon rainforest are formed by the oxidation of biogenic volatile organic compounds  
206 (Jimenez et al., 2009; Hallquist et al., 2009; Martin et al., 2010a) and are the major constituents of  
207 particulate matter (PM), particularly for submicron ambient PM (Pöschl, et al., 2010; Martin et al.,  
208 2010b; Chen et al., 2015). In the SEI images, pure SOA droplet particles appear gray in contrast  
209 and have a circular shape, as shown in Fig. 6(a). As TEM grid films (with 90% C content) and  
210 SOAs are composed mainly of carbon and oxygen, the SOA aerosols appear gray on the TEM  
211 grids because of their similar secondary and backscattered electron yields to those of the TEM grid



212 (Goldstein et al., 2003; Maskey et al., 2010). As TEM grids are hydrophobic due to the thin carbon  
213 layer over the Formvar film, the aqueous droplet aerosols appear circular on the TEM grids (Eom  
214 et al., 2014; Maskey et al., 2010), suggesting that SOAs were collected as aqueous droplets at the  
215 time of particle sample collection. Recent studies also reported that most submicron SOA particles  
216 in the Amazon basin are water soluble organic aerosols (WSOAs) rather than semi-solid or solid  
217 aerosols under the background conditions that are typically met during the wet season (Bateman  
218 et al., 2016, 2017). The X-ray spectrum of a typical pure SOA, as shown in Fig. 6(a), showed  
219 considerably higher levels of the C X-ray peak intensity compared to that from the Formvar/carbon  
220 film of the TEM grids, resulting in the unambiguous identification of SOA particles based on their  
221 SEIs and X-ray spectral data.

222

### 223 3.1.2. Ammonium sulfate (AS) particles

224 Ammonium sulfate particles were observed abundantly in the ATTO and Manaus samples,  
225 mostly as mixtures with secondary organics. Ammonium sulfate particles appear bright and  
226 crystalline on the SEIs before the X-ray measurements, both for pure airborne and standard  
227 ammonium sulfate particles, as shown in Figs. 6(b) and 6(f), respectively. The standard ammonium  
228 sulfate particles were deposited on TEM grids by the nebulization of a 0.1 M ammonium sulfate  
229 solution. As shown in the inset in Figs. 6(b) and 6(f), after the X-ray measurements, they show  
230 somewhat darkened SEIs with black holes, due to electron beam damage, at the places where the  
231 electron beam hits. As the ammonium sulfate particles are electron beam-sensitive (Geng et al.,  
232 2010; Worobiec et al., 2003; Huang and Turpin, 1996), their X-ray spectral signature is the  
233 presence of a significant S X-ray peak, as shown for both pure airborne and standard particles on  
234 the TEM grids. The N X-ray peak was often not detected, particularly for small particles because  
235 the  $\text{NH}_4^+$  moiety is especially prone to damage by electron beams.

236 Ambient urban and rural sulfates act as a sink for ammonia, of which the sources are largely  
237 animal waste, fertilizer application, soil release, and industrial emissions. The most common form  
238 is ammonium sulfate. On the other hand, if ammonia is scarce in the air, sulfates would be in more  
239 acidic forms, such as  $\text{NH}_4\text{HSO}_4$  or  $\text{H}_2\text{SO}_4$  (Millstein et al., 2008). The acidic  $\text{NH}_4\text{HSO}_4/\text{H}_2\text{SO}_4$   
240 particles have been reported to be more hygroscopic than pure ammonium sulfate (Pósfai et al.,  
241 1998). Hence, they can be spread over the collecting substrate (Formvar/carbon film). In addition,  
242 acidic sulfate particles can have unique halo rings in their morphology (Buseck and Pósfai, 1999).





243 The crystalline structure of the ammonium sulfate-containing particles observed in this study  
244 suggests that they are sulfates fully neutralized with ammonia. In addition, the Raman spectra of  
245 airborne particles exhibiting this morphology were obtained on a single particle basis to confirm  
246 that they are ammonium sulfate. As shown in Fig. 7(a), the Raman peak at  $975\text{ cm}^{-1}$  of the airborne  
247 particle is characteristic of ammonium sulfate (Ling and Chan, 2007), which was also confirmed  
248 by Raman spectroscopy on standard ammonium sulfate particles. Characteristic Raman peaks for  
249  $\text{NH}_4\text{HSO}_4$ ,  $\text{K}_2\text{SO}_4$ ,  $\text{CaSO}_4\cdot 2\text{H}_2\text{O}$ ,  $\text{CaSO}_4$ ,  $\text{Na}_2\text{SO}_4$ , and  $\text{MgSO}_4\cdot x\text{H}_2\text{O}$  ( $x = 1-7, 11$ ) were reported  
250 to be at 1010 and 1042, 983, 1008, 1014 and 1025, 992, and 984-1046  $\text{cm}^{-1}$ , respectively (Fung  
251 and Tang, 1988; Wang et al., 2006; Mabrouk et al., 2013; Prieto-Taboada et al., 2014). The sloping  
252 baseline in the Raman spectrum of the airborne particle was attributed to the fluorescence from  
253 organics, indicating the presence of organic compounds (Sobanska et al., 2012), probably from  
254 SOA. For aerosols collected on Ag foil at the ATTO site on June 10, 2014, ammonium sulfate is  
255 the major species with some organics and minerals such as kaolinite, for the bulk aerosols in the  
256 size range of  $0.25 - 0.5\ \mu\text{m}$ , based on their X-ray, attenuated total reflectance-FTIR (ATR-FTIR),  
257 and Raman spectra (Fig. 7(b)). A study of the samples collected in the central Amazon Basin during  
258 the wet season from February to March 2008 reported that ammonium was not sufficient to fully  
259 neutralize sulfates so that ammonium bisulfate would be present in the Amazon rainforest (Chen  
260 et al, 2015), whereas other studies reported that sulfates are sufficiently neutralized with ammonia  
261 in the fine and coarse fractions during both the wet and dry seasons (Andreae et al., 2015; Martin  
262 et al., 2010b; Fuzzi et al., 2007; Mace et al., 2003). The different results may be due to different  
263 sampling places and seasons. In this study, ammonium sulfate is dominant over ammonium  
264 bisulfate.

265 Previous studies have shown that the sulfate aerosols over the Amazon forest are  
266 predominantly from marine and terrestrial biogenic sources, with comparable contributions from  
267 marine and terrestrial biogenic emissions (Andreae et al., 1990). Sulfate originates from biogenic  
268 sources in the rainforest, i.e., dimethyl sulfide (DMS),  $\text{H}_2\text{S}$ , and  $\text{CS}_2$  emitted by plants and  
269 microorganisms, which can be oxidized to sulfate (Andreae et al., 1990, 2015; Martin et al., 2010b).  
270 The rainforest ecosystem in the central Amazon can act as a source of DMS to the atmosphere  
271 throughout the year (Jardine et al., 2015). Several studies have reported that marine DMS  
272 transported from the Atlantic Ocean contributes significantly to the sulfate levels in the Amazon  
273 basin (Gregory et al., 1986; Andreae et al., 1990; Martin et al., 2010a). In addition, there is some



274 sulfate from long-range transport across the Atlantic and minor upwind anthropogenic sources.

275 The nitrogen cycle is essential for organisms and some bacteria to fix the gaseous  $N_2$  in the  
276 air to  $NH_4^+$  for their own biosynthetic processes (Kim and Rees, 1994; Bazzaz, 1998; Kellerhals  
277 et al., 2010). In addition, some microorganisms produce enzymes to release nitrogen as  $NH_4^+$   
278 during the nitrogen mineralization process, which is important in tropical rain forest soils, where  
279 dead plants and animal matter accumulate continuously (Wright, 1996; Neill et al., 1999). A high  
280 level of  $NH_4^+$  in tropical rain contributes significantly to the nitrogen influx in the rainforest soils  
281 (Jordan et al., 1982). The  $NH_4^+$  species can be evaporated as gaseous  $NH_3$  from surface soils,  
282 particularly from leaf litter, resulting in a strong  $NH_3$  emission source as well as stomatal  $NH_3$   
283 emission of plants as another natural source in forest ecosystems (Sutton et al., 2009, 2013; Hansen  
284 et al., 2017). On the other hand,  $NH_4^+$  species in rainforest soils might become airborne  
285 immediately after rainfall, similar to the way that airborne organic particles are produced directly  
286 from soils by raindrop impaction (Wang et al., 2016). The wetness of forest surfaces is significant  
287 in controlling both the deposition and emission of atmospheric  $NH_3$  (Hansen et al., 2015). As  
288 ammonium sulfate-containing particles were also observed abundantly in the samples collected at  
289 Manaus site, they were influenced strongly by the surrounding Amazonian forest and/or generated  
290 by anthropogenic activities in the urban environment.

291

### 292 3.1.3. SOA and AS mixture particles

293 In this study, most airborne submicron SOAs were observed to be internally mixed with  
294 ammonium sulfate, particularly for the samples collected at the ATTO site. Figure 6(c) shows that  
295 a typical SOA and AS mixture particle has the crystalline, bright ammonium sulfate moiety in the  
296 center surrounded by circular, grey organic species. The circular morphology of the organic species  
297 strongly suggests that the organic species are SOAs, as stated above. As efflorescence and  
298 deliquescence relative humidity (ERH and DRH) of ammonium sulfate species are 30-40% and  
299 80%, respectively (Yeung and Chan, 2010) and the ambient RH was always above 55% during  
300 sampling for the ATTO and Manaus samples, the ammonium sulfate would be mostly in aqueous  
301 droplets at the time of sample collection, rather than in crystalline form, as indicated by their  
302 overall circular shape. When the particle samples were under dry conditions either during sample  
303 storage or in the vacuum chamber of the SEM instrument, the ammonium sulfate species  
304 crystallized, resulting in core-shell structures of organic and inorganic mixture aerosols. When the



305 ambient RH is low enough to make the ammonium sulfate species crystallize in the atmosphere,  
306 the organic and inorganic mixture aerosols would similarly be present as core-shell structures.

307 Some of the SOA and AS mixture particles were also mixed with K-salts. As shown in Figs.  
308 6(d) and 6(e), their morphology was similar to that of the SOA and AS mixture particles, but their  
309 X-ray spectra revealed the presence of K and an elevated S level compared to those of the SOA  
310 and AS mixture particles, suggesting that the K is associated mostly with  $\text{SO}_4^{2-}$ . The shoulder  
311 Raman peak of the airborne ammonium sulfate particle at  $982\text{ cm}^{-1}$  (Fig. 7(a)), which is indicative  
312 of the  $\text{K}_2\text{SO}_4$  moiety (Mabrouk et al., 2013), also suggests that the K-salts are most probably  $\text{K}_2\text{SO}_4$ .  
313 A previous study reported that small K-salt-rich particles can act as seeds for SOA formation in  
314 the Amazon basin and K-salts are present ubiquitously in Amazonian SOAs with their content  
315 being higher in the morning hours and for smaller SOAs (Pöhlker et al., 2012). On the other hand,  
316 among the 843 submicron SOA and/or ammonium sulfate particles collected at the ATTO site,  
317 only 31% contained K-salts, which is probably because the samples were collected in the afternoon  
318 and/or the analyzed particles were larger than  $0.25\text{ }\mu\text{m}$  so that the K-salt content may be below the  
319 detection limit of EDX ( $\sim 0.1\text{ wt. }\%$ ). In the Manaus samples, a total of 199 submicron SOA and/or  
320 ammonium sulfate particles were observed, of which approximately 40% contained K-salts,  
321 suggesting that the Manaus samples were influenced strongly by the surrounding rainforest as  
322 supported by the backward trajectories (Figs. 2(e)-(g)), where K-salts may be mostly of a biogenic  
323 origin in the rainforest. The organic moiety is often mixed internally with aged sea-salts, mineral  
324 dust, and PBAs, which will be described below.

325

#### 326 **3.1.4. Mineral dust particles**

327 The typical mineral dust particles include aluminosilicate, quartz ( $\text{SiO}_2$ ), calcite ( $\text{CaCO}_3$ ),  
328 dolomite ( $\text{CaMg}(\text{CO}_3)_2$ ), and  $\text{TiO}_2$  (Geng et al., 2009, 2011). They appear irregular and bright on  
329 the SEIs (Fig. 8). Various types of mineral particles from Saharan dust contribute significantly to  
330 the nutrient cycles in the Amazon rainforest (Talbot et al., 1990; Abouchami et al., 2013; Rizzolo  
331 et al., 2017). Mineral dust tends to provide reactive surfaces for heterogeneous reactions with trace  
332 atmospheric gases, such as  $\text{SO}_2$  and  $\text{NO}_x$ , leading to chemical modifications of the particles that  
333 ultimately affect the atmospheric chemical balance and photochemical cycle (Sullivan et al., 2007;  
334 Chen et al., 2011). Modification of the physicochemical properties of particles can alter their  
335 optical, chemical, and hygroscopic properties (Sullivan et al., 2007; Geng et al., 2014). If some



336 components in them (particularly Ca-containing species) react with airborne SO<sub>2</sub> and NO<sub>x</sub> in the  
337 presence of moisture or with “secondary acids”, such as H<sub>2</sub>SO<sub>4</sub>, HNO<sub>3</sub>, and HCl, they are regarded  
338 as reacted or aged ones. The reacted/aged ones can contain either nitrates, sulfates, or both (Geng  
339 et al., 2014, 2017). In the Amazon samples, almost all the mineral dust particles were aged ones,  
340 as shown in Fig. 8, where an aluminosilicate and a carbonate/silica mixture particle containing  
341 sulfate are shown. The S-containing aged mineral dust particles outnumbered the N- and both N-  
342 and S-containing ones for the ATTO samples, whereas they were comparable to both the N- and  
343 S-containing ones for the Manaus samples, as shown in Fig. 9(a), indicating the predominance of  
344 sulfates over nitrates for the reaction of mineral dust particles at the ATTO site and somewhat  
345 significant influence of nitrates at the Manaus site. The mineral particles might be mixed or  
346 covered with SOA and/or ammonium sulfate and gradually become aged under a high RH in the  
347 rainforest. Some mineral particles were also mixed with sea salt particles during their transport to  
348 the Amazonian area across the Atlantic Ocean.

349

### 350 **3.1.5. Reacted (aged) sea-salts**

351 The nascent airborne sea-salt particles can react with gas-phase sulfur and nitrogen oxides  
352 to contain sulfate and nitrate, respectively (ten Brink, 1998). During the process, chlorine may be  
353 removed completely if the reaction is complete (Laskin et al., 2003). All sea-salt particles observed  
354 in the ATTO and Manaus samples were reacted ones. Figure 10(a) shows the X-ray spectrum,  
355 atomic concentration, and SEI of a typical aged sea salt particle, where the presence of Na, Mg,  
356 and Cl indicates its marine origin (Geng et al., 2014) and the presence of S and C indicates that it  
357 is mixed with sulfates and organics. The irregular and somewhat bright SEI is typical of the aged  
358 sea-salt particles. As shown in Fig. 9(b), S-containing sea-salts outnumbered N- and both N- and  
359 S-containing ones for the ATTO samples, indicating the predominance of sulfates over nitrates for  
360 the reaction of sea-salt particles. The S-containing particles are comparable in abundance to both  
361 the N- and S-containing ones at the Manaus site (Fig. 9(b)). The sea-salt particles may also become  
362 mixed with ammonium sulfate over the rainforest and become S-containing ones. Among overall  
363 275 reacted sea-salts containing sulfate/nitrate and organics, 71% of them were mixed with K-salts,  
364 as shown in Fig. 10(b). The presence of K-salts in the reacted sea-salt particles indicates that the  
365 mixing of the K-salts of biogenic origin would happen in the rainforest during long-range transport  
366 because of the minimal biomass burning influence during the wet season. In addition, several



367 elongated  $\text{CaSO}_4$  particles, as shown in Fig. 10(c), were detected in both ATTO and Manaus  
368 samples, all of which contain a small amount of Na. Their elongated shape and the presence of Na  
369 strongly indicates that they were from the sea, possibly the Atlantic Ocean, not from the soil (Eom  
370 et al., 2016).

371

### 372 **3.1.6. Primary biological aerosol (PBA) particles**

373 PBA particles like fungal spores can be identified easily based on their unique morphology  
374 and the presence of their characteristic chemical elements (Geng et al., 2009; Martin et al, 2010a;  
375 Pöschl et al., 2010). The PBA particle shown in Fig. 11(a) has a unique oval morphology and the  
376 majority of C together with the characteristic small amounts of N, P, S, Cl, and K. PBA particles  
377 are relatively large (size  $> 2.0 \mu\text{m}$ ) so that they are abundant in stage 4 samples ( $2.0 \mu\text{m} < \text{size} <$   
378  $4.0 \mu\text{m}$ ), particularly at the ATTO site. Figure 12 shows two image fields of stage 4 samples  
379 collected at the ATTO and Manaus sites, where the PBA particles have various types of  
380 morphology and many of them are mixed with SOA. The abundant observation of PBA particles  
381 in the stage 4 sample of the Manaus site suggests the transport of the PBA particles from the  
382 rainforest to the urban area. Supermicron PBA particles were reported to be abundant over the  
383 Amazon (China et al., 2016; Moran-Zuloaga et al., 2017; Gilardoni et al., 2011). PBA particles can  
384 be pollen, bacteria, fungal and fern spores, viruses, and fragments of plants and animals emitted  
385 directly from the rainforest, showing a range of morphologies, and comprise the largest fraction of  
386 the coarse mass (Martin et al, 2010a). PBA particles appear to be the most efficient and abundant  
387 ice nuclei (Pöschl et al., 2010; Tobo et al., 2013; Haga et al., 2014). In addition, the release of  
388 nano- and submicron particles from fungal spores under high relative humidity can contribute to  
389 new particle formation and potentially affect cloud formation in the Amazon Basin (China et al.,  
390 2016).

391

### 392 **3.1.7. Carbon-rich particles from combustion sources**

393 Carbon-rich particles, such as soot, tar balls, and char or coal dust, which contain more  
394 than 90 at. % C and O with the C content being dominant over O in low-Z particle EPMA analysis  
395 (Geng et al., 2009, 2010, 2014), were observed frequently in the Manaus samples, whereas they  
396 were rare in the ATTO samples. Based on the characteristic morphology of carbon-rich particles,  
397 soot aggregates of fractal-like chain structures (Fig. 11(b)), tar balls of separate spherules (Fig.



398 11(c)), and chars of irregular-shaped carbon (Fig. S5, SM1-2) could be differentiated  
399 straightforwardly from each other (Geng et al., 2010, 2014). The soot aggregates formed via a  
400 vaporization-condensation mechanism during the combustion processes vary in size from sub to  
401 several micrometers (Chen et al., 2005, 2006). Once airborne, the complex microstructure of the  
402 soot aggregates may provide active sites for the deposition of organics and other chemical species,  
403 such as sulfates (Pósfai et al., 1999; Zhang et al., 2008), as revealed by the presence of S in Fig.  
404 11(b). This results in aged soot aggregates that become compact with considerable restructuring  
405 and shrinkage (Zhang et al., 2008). Tar balls, which are a type of brown carbon, usually have high  
406 C, N, and O contents with a spherical morphology (Fig. 11(c)), strongly indicating their formation  
407 during biomass combustion processes (Pósfai et al., 2003, 2004). Char appears compact and  
408 irregular in the SEIs; it is often mixed with minor inorganic species, such as K and S, and is  
409 regarded as the incomplete combustion remnants of liquid or solid carbonaceous fuel materials  
410 that have undergone carbonization during combustion (Chen et al., 2006). Only one soot particle  
411 was observed in all the ATTO samples, whereas soot, tar ball, and char or coal dust particles were  
412 abundant in the submicron Manaus samples, suggesting that the ATTO samples are barely affected  
413 by the anthropogenic carbon-rich particles generated in Manaus.

414

### 415 **3.1.8. Fly ash particles**

416 As shown in Fig. 11(d), fly ash particles are glassy spheres, composed mainly of O, Si, and  
417 Al with minor components, such as Fe and Ca, which can be identified clearly by their spherical  
418 shape and bright contrast on SEIs. The fly ash particles are different from tar balls having only C  
419 and O signals in their X-ray spectra, even though both are generated during the combustion  
420 processes (Geng et al., 2017). They were observed only in the Manaus samples, reflecting their  
421 anthropogenic origin.

422

### 423 **3.1.9. Heavy metal-containing particles**

424 Heavy metal-containing (HM) particles, such as Ni-, Ti-, Zn-, and Fe-containing ones,  
425 appear bright and irregular on SEM images, as shown in Figs. 11(e) and (f), and were observed  
426 mostly in the fine fraction with more than a half of them being Fe-containing particles both in the  
427 ATTO and Manaus samples. The Fe-containing particles in the ATTO samples were observed to  
428 be associated with SOA (and ammonium sulfate), as shown in Fig 11(f), indicating its mixing with



429 the species of a biogenic emission origin. Sahara mineral dust has been reported to be essential for  
430 the nutrient cycles in the Amazon rainforest because many types of minerals are carried and  
431 transported into the rainforest, in which Fe is one of the important micronutrients in a Fe-limited  
432 rainforest (Rizzolo et al., 2017). Among all the mineral dust particles observed in the samples,  
433 approximately 40% of them contain Fe. The HM particles can also be of anthropogenic origin:  
434 emitted from the streets or road surface as brake dust, road paint particles, diesel exhaust particles,  
435 construction materials, and/or car catalyst materials (Qiao et al., 2016).

436

### 437 **3.2. Relative abundances of particle types observed in the ATTO and Manaus samples**

438 Figure 13 shows the relative abundance of the nine different particle types observed in the  
439 ATTO and Manaus samples. In the stage 1 samples (0.25-0.5  $\mu\text{m}$  size) of SA1-SA4 collected at  
440 the ATTO site, almost all the particles were SOA and AS mixtures (> 93%). In the stage 2 samples  
441 (0.5-1.0  $\mu\text{m}$  size), SOA and AS mixture particles were dominant for the SA2 and SA3 samples  
442 (94% and 82%, respectively). In the stage 2 samples of samples SA1 and SA4, SOA and AS  
443 mixture particles were most abundant (50% and 58%, respectively), followed by pure ammonium  
444 sulfates (12% and 18%, respectively), aged mineral dust (19% and 8%, respectively), and pure  
445 SOA particles (11% and 6%, respectively). In the stage 2 samples of SA1-SA4, the summed  
446 contents of SOA and ammonium sulfate were 73%, 99%, 85%, and 82%, respectively, suggesting  
447 that SOA and AS are the predominant species in submicron aerosols collected at the ATTO site.  
448 The observation of abundant submicron SOAs, which constitute a significant fraction of fine  
449 aerosol mass during the wet season at the rainforest, has been reported (Chen et al., 2015; Gilardoni  
450 et al., 2011). SOA particles are formed through atmospheric oxidation, condensation, and the gas-  
451 to-particle conversion of biogenic volatile organic compounds, such as isoprene and terpenes  
452 emitted from the rainforest (Pöschl et al., 2010; Gilardoni et al., 2011; Andreae et al., 2015;  
453 Andreae et al., 2018). Although ammonium sulfates were reported to be present in significant  
454 quantities in the Amazon basin (Andreae et al., 2015; Chen et al., 2015; Fraund et al., 2017), this  
455 study emphasizes the observation of the predominant submicron ammonium sulfates mixed with  
456 SOA.

457 In the stage 2 samples, aged mineral dust and sea-salts (19% and 4%) for the SA1 sample,  
458 reacted sea salts (11%) for the SA3 sample, and aged mineral dust and sea-salts (8% and 5%) for  
459 the SA4 sample were observed, suggesting that the samples from outside the Amazon rainforest



460 have different influences because the mineral dust and sea-salt particles were all aged ones. The  
461 influences from outside were observed more clearly for supermicron aerosols at the ATTO site. In  
462 the stage 3 samples (1.0-2.0  $\mu\text{m}$  size) of SA1-SA4, reacted sea-salt particles (33%, 34%, 30%, and  
463 36%, respectively) and aged mineral dust particles (37%, 11%, 7%, and 10%, respectively) were  
464 abundantly observed although the summed relative abundances of SOA and ammonium sulfate  
465 were 28%, 43%, 58%, and 50%, respectively, indicating that SOA and ammonium sulfate are  
466 abundant even in supermicron ATTO aerosols. As all the mineral dust particles were aged, they are  
467 not of local origin, and the observation of a high content (37%) of aged mineral dust particles in  
468 sample SA1 highlights the importance of long-range transatlantic transport (see the fast-moving  
469 air-masses from the Atlantic Ocean for the SA1 sample (Fig. 2(a)). Many studies have examined  
470 the influence of the Saharan dust particles over the Amazon rainforest region, starting with the  
471 measurements made during the ABLE-2B campaign (Talbot et al., 1990; Swap et al., 1992).  
472 Mineral dust is imported most frequently to the rainforest in March and April (Martin et al., 2010a;  
473 Moran-Zuloaga et al., 2018), which increases the ground-based soil dust element levels  
474 significantly (Artaxo et al., 2013). The dust particles can act as ice nuclei and facilitate cold rain  
475 formation (Pöschl et al., 2010). Volatile organic compounds and secondary organics can also  
476 condense on the sea-salt and mineral particles, and the secondary organic coating on the mineral  
477 dust and sea-salt particles can modify their optical, chemical, and hygroscopic properties  
478 significantly (Pöschl et al., 2010; Geng et al., 2014). For example, soluble organic material  
479 coatings on the dust particles may reduce their original ice-nucleating ability and enhance their  
480 cloud-nucleating ability (Tobo et al., 2010; Manktelow et al., 2010). In this study, approximately  
481 70% and 90% of the reacted sea-salt/mineral dust particles in the ATTO and Manaus samples,  
482 respectively, were either mixed or coated with organic matter in the Amazon basin and/or during  
483 the long-range transport.

484 PBA particles, which are from the rainforest, are sometimes observed in the stage 3 samples  
485 (2%, 10%, 3%, and 3% for the SA1-SA4 samples, respectively). In the stage 4 sample (2.0-4.0  $\mu\text{m}$   
486 size) of the SA4 sample, the most abundant particle type was PBA (46%), followed in order by  
487 reacted sea-salt (28%), SOA (12%), aged mineral dust (9%), and ammonium sulfate (4%), where  
488 both PBA, SOA, and ammonium sulfate particles of a local origin and the reacted sea-salt and  
489 mineral dust particles from the outside are considerably present. In summary, the aerosols collected  
490 at the ATTO site are mostly SOA and ammonium sulfate of a local origin in the submicron fraction,





491 although some of the submicron sulfate are of marine and distant origin, whereas aerosols of both  
492 local and distant origins are significant in the supermicron fraction.

493 The aerosols collected at the Manaus site were diverse compared to those at the ATTO site.  
494 As shown in Fig. 13, for the stage 1 samples, SOA and ammonium sulfate particles, including their  
495 mixture, were the major components for the SM1 and SM2 samples (66% and 62%, respectively),  
496 whereas they were only 17% for the SM3 sample. For the stage 2 samples, they were 80%, 53%,  
497 and 25% for the SM1-SM3 samples, respectively. As SOA and ammonium sulfate particles can be  
498 from the surrounding rainforest areas in addition to local anthropogenic sources, samples SM1-  
499 SM3 collected at the Manaus site appear to be influenced from the outside in the order of samples  
500 SM1 > SM2 > SM3. In addition, considerable amounts of submicron carbonaceous particles were  
501 observed, such as soot, char, and tar balls, which are of a local origin (for the SM1-SM3 samples,  
502 21%, 25%, and 78% for stage 1 and 6%, 29%, and 49% for stage 2, respectively). The most  
503 abundant submicron aerosols for sample SM3 were carbonaceous ones, indicating that the local  
504 influence to the samples is in the order of SM3 > SM2 > SM1.

505 In supermicron Manaus aerosols, PBA particles, aged mineral dust, and reacted sea-salts in  
506 addition to SOA and carbonaceous particles are abundant. In the stage 3 aerosols of the SM1  
507 sample, the most abundant particles were reacted sea-salts, followed by aged mineral dust, SOA,  
508 ammonium sulfate, and PBA particles, which also indicates the strong influence on the SM1  
509 sample from the outside. In stage 3 aerosols of the SM2 sample, the most abundant particles were  
510 SOA, followed in order by aged mineral dust, reacted sea-salt, PBA, carbonaceous particles, and  
511 ammonium sulfate, which also indicates the strong influence on the SM2 sample from the  
512 surrounding rainforest areas. In the stages 3 and 4 aerosols of the SM3 sample, the most abundant  
513 particles were aged mineral dust (36% and 52% for stages 3 and 4, respectively), followed by  
514 carbonaceous particles, PBA, SOA, and reacted sea-salt. As the aged sea-salt contents were  
515 relatively low (10% and 4% for stages 3 and 4, respectively), most of the aged mineral dusts appear  
516 to be of a local origin. Fly ash and heavy metal-containing particles of an anthropogenic local  
517 origin were considerable in the Manaus samples, i.e., they were observed in the range of 3-7%  
518 relative abundances in the Manaus samples. In particular, soot particles of an anthropogenic origin  
519 were observed ubiquitously in all the Manaus samples. Among the samples, the aerosols collected  
520 at the Manaus site were different. The SM1 sample was influenced most strongly from the outside,  
521 including the surrounding rainforest and transatlantic transport. The SM2 sample has some



522 influences by local sources as well as from the outside. The SM3 sample contains mainly aerosols  
523 of an anthropogenic local origin in the submicron fraction and some influences from the outside  
524 in the supermicron fraction. Figures 2(e)-(f) show that the backward trajectories at heights of 100-  
525 m and 500-m are further from the outside in the order of SM1 > SM2 > SM3, which is consistent  
526 with the characteristics of submicron and supermicron aerosols of the SM1-SM3 samples.

527

## 528 Conclusions

529 In this study, aerosol samples collected in the Amazonian rainforest and Manaus, Brazil  
530 during the 2012 wet season were investigated on a single particle basis using low-Z particle EPMA.  
531 The aerosol particles were classified into nine particle types based on their morphology on SEIs  
532 together with the elemental concentrations of a total of 3,162 individual particles: (i) secondary  
533 organic aerosols (SOA), (ii) ammonium sulfate (AS) particles, (iii) SOA and AS mixture particles,  
534 (iv) aged mineral dust, (v) reacted sea-salts, (vi) primary biological aerosol (PBA) particles, (vii)  
535 carbon-rich or elemental carbon (EC) particles such as soot, tar ball, and char, (viii) fly ash particles,  
536 and (ix) heavy metal (HM, such as Fe, Zn, Ni, and Ti)-containing particles. For submicron aerosols  
537 collected at the ATTO site, the SOA and AS mixture particles were predominant (50-94% in  
538 relative abundance) with the summed contents of SOA and ammonium sulfate being 73-100%. In  
539 contrast, in the supermicron aerosols at the ATTO site, aged mineral dust and sea-salt (37-70%) as  
540 well as SOA and ammonium sulfate (28-58%) were abundant. PBAs were observed abundantly in  
541 the PM<sub>2.4</sub> fraction (46%), and EC and fly ash particles were absent in all the fractions. An analysis  
542 of a bulk PM<sub>0.25-0.5</sub> aerosol sample collected at the ATTO site using RMS and ATR-FTIR showed  
543 that ammonium sulfate, organics, and minerals are the major chemical species, which is consistent  
544 with the EPMA results.

545 In the submicron aerosols collected in Manaus, either SOA and ammonium sulfate (17-  
546 80%) or EC particles (6-78%) were dominant, depending on the samples. The supermicron  
547 aerosols collected in Manaus consisted mainly of aged mineral dust, reacted sea-salts, PBA, SOA,  
548 ammonium sulfate, and EC particles. SOA, ammonium sulfate, and PBAs were mostly of a  
549 biogenic origin and EC and HM-containing particles were of an anthropogenic origin. The aged  
550 mineral dust and reacted sea-salt particles, including mineral dust mixed with sea-salts probably  
551 during long-range transatlantic transport, were abundant in the supermicron fractions at both sites.  
552 The submicron aerosol at the ATTO site was influenced mainly by the emission from the rainforest



553 and its supermicron aerosols showed additional contributions from long-range transport, including  
554 the Atlantic Ocean and Sahara desert, whereas the aerosols collected in Manaus showed different  
555 local and outside contributions among the samples. Among all the aged mineral dust and reacted  
556 sea-salt particles, sulfate-containing ones outnumbered those containing nitrates and both nitrate  
557 and sulfate in the ATTO samples, whereas N and S containing particles were comparable to sulfate-  
558 only ones in the Manaus samples, indicating the different sources and formation mechanisms of  
559 secondary aerosols, i.e., the predominant presence of sulfate at the ATTO site from biogenic  
560 emissions and elevated influences of nitrates from anthropogenic activities at the Manaus site.

561

#### 562 **Author contributions**

563 LW, RHMG, and CR designed the experiment and LW, XL, and HKK carried out the  
564 measurements and analyzed the data. CGGB, CIY, RAFDS, and CP organized and performed the  
565 samplings. LW, HG, RHMG, CGGB, AFLG, and CR interpreted the observations and LW, HG,  
566 RHMG, CGGB, MOA, and CR drafted the paper.

567

#### 568 **Acknowledgement**

569 This study was supported by Basic Science Research Programs through the National Research  
570 Foundation of Korea (NRF) funded by the Ministry of Education, Science, and Technology (NRF-  
571 2018R1A2A1A05023254). The work of M. O. Andreae and C. Pöhlker was supported by the  
572 German Max Planck Society (MPG). For the operation of the ATTO site, we acknowledge the  
573 support by the German Federal Ministry of Education and Research (BMBF contract 01LB1001A),  
574 the Brazilian Ministério da Ciência, Tecnologia e Inovação (MCTI/FINEP contract  
575 01.11.01248.00), and the Coordination for the Improvement of Higher Education Personnel  
576 (CAPES) for scholarship funding (investigation ) as well as the Amazon State University (UEA),  
577 FAPEAM, LBA/INPA, and SDS/CEUC/RDS-Uatumã. A special thanks to Claudomiro Mauricio  
578 da Silva for the support during sampling.

579

#### 580 **References**

581 Abouchami, W., Nätke, K., Kumar, A., Galer, S. J. G., Jochum, K. P., Williams, E., Horbe, A. M.  
582 C., Rosa, J. W. C., Balsam, W., Adams, D., Mezger, K., and Andreae, M. O., Geochemical  
583 and isotopic characterization of the Bodélé Depression dust source and implications for



- 584 transatlantic dust transport to the Amazon Basin, *Earth Planet. Sci. Lett.*, 380, 112-123,  
585 doi:10.1016/j.epsl.2013.08.028, 2013.
- 586 Andreae, M. O.: Aerosols before pollution, *Science*, 315, 50–51, doi:10.1126/science.1136529,  
587 2007.
- 588 Andreae, M. O., Berresheim, H., Bingemer, H., Jacob, D. J., Lewis, B. L., Li, S.-M., and Talbot,  
589 R. W.: The atmospheric sulfur cycle over the Amazon Basin, 2. Wet Season, *J. Geophys. Res.*,  
590 95, 16813–16824, doi:10.1029/JD095iD10p16813, 1990.
- 591 Andreae, M. O., Acevedo, O. C., Araùjo, A., Artaxo, P., Barbosa, C. G. G., Barbosa, H. M. J., Brito,  
592 J., Carbone, S., Chi, X., Cintra, B. B. L., da Silva, N. F., Dias, N. L., Dias-Júnior, C. Q., Ditas,  
593 F., Ditz, R., Godoi, A. F. L., Godoi, R. H. M., Heimann, M., Hoffmann, T., Kesselmeier, J.,  
594 Könemann, T., Krüger, M. L., Lavric, J. V., Manzi, A. O., Lopes, A. P., Martins, D. L.,  
595 Mikhailov, E. F., Moran-Zuloaga, D., Nelson, B. W., Nölscher, A. C., Santos Nogueira, D., T.  
596 F. Piedade, M., Pöhlker, C., Pöschl, U., Quesada, C. A., Rizzo, L. V., Ro, C.-U., Ruckteschler,  
597 N., Sá, L. D. A., de Oliveira Sá, M., Sales, C. B., dos Santos, R. M. N., Saturno, J., Schöngart,  
598 J., Sörgel, M., de Souza, C. M., de Souza, R. A. F., Su, H., Targhetta, N., Tóta, J., Trebs, I.,  
599 Trumbore, S., van Eijck, A., Walter, D., Wang, Z., Weber, B., Williams, J., Winderlich, J.,  
600 Wittmann, F., Wolff, S., and Yáñez-Serrano, A. M.: The Amazon Tall Tower Observatory  
601 (ATTO): overview of pilot measurements on ecosystem ecology, meteorology, trace gases,  
602 and aerosols, *Atmos. Chem. Phys.*, 15, 10723–10776, doi:10.5194/acp-15-10723-2015, 2015.
- 603 Andreae, M. O., Afchine, A., Albrecht, R., Holanda, B. A., Artaxo, P., Barbosa, H. M. J., Borrmann,  
604 S., Cecchini, M. A., Costa, A., Dollner, M., Fütterer, D., Järvinen, E., Jurkat, T., Klimach, T.,  
605 Konemann, T., Knote, C., Krämer, M., Krisna, T., Machado, L. A. T., Mertes, S., Minikin, A.,  
606 Pöhlker, C., Pöhlker, M. L., Pöschl, U., Rosenfeld, D., Sauer, D., Schlager, H., Schnaiter, M.,  
607 Schneider, J., Schulz, C., Spanu, A., Sperling, V. B., Voigt, C., Walser, A., Wang, J., Weinzierl,  
608 B., Wendisch, M., and Ziereis, H.: Aerosol characteristics and particle production in the upper  
609 troposphere over the Amazon Basin, *Atmos. Chem. Phys.*, 18, 921-961, doi:10.5194/acp-18-  
610 921-2018, 2018.
- 611 Artaxo, P., Fernandes, E. T., Martins, J. V., Yamasoe, M. A., Hobbs, P. V., Maenhaut, W., Longo,  
612 K. M., and Castanho, A.: Large-scale aerosol source apportionment in Amazonia, *J. Geophys.*  
613 *Res.*, 103(D24), 31837–31847, doi:10.1029/98JD02346, 1998.
- 614 Artaxo, P., Rizzo, L. V., Brito, J. F., Barbosa, H. M., Arana, A., Sena, E. T., Cirino, G. G., Bastos,



- 615 W., Martin, S. T., Andreae, M., O.: Atmospheric aerosols in Amazonia and land use change:  
616 from natural biogenic to biomass burning conditions, *Faraday Discuss.*, 165, 203-235, doi:  
617 10.1039/C3FD00052D, 2013.
- 618 Bateman, A. P., Gong, Z., Liu, P., Sato, B., Cirino, G., Zhang, Y., Artaxo, P., Bertram, A. K., Manzi,  
619 A. O., Rizzo, L. V., Souza, R. A. F., Zaveri, R. A., and Martin, S. T.: Sub-micrometre  
620 particulate matter is primarily in liquid form over Amazon rainforest, *Nat. Geosci.*, 9, 34–37,  
621 doi:10.1038/ngeo2599, 2016.
- 622 Bateman, A. P., Gong, Z., Harder, T. H., de Sá, S. S., Wang, B., Castillo, P., China, S., Liu, Y.,  
623 O'Brien, R. E., Palm, B. B., Shiu, H.-W., Cirino, G. G., Thalman, R., Adachi, K., Alexander,  
624 M. L., Artaxo, P., Bertram, A. K., Buseck, P. P., Gilles, M. K., Jimenez, J. L., Laskin, A.,  
625 Manzi, A. O., Sedlacek, A., Souza, R. A. F., Wang, J., Zaveri, R., and Martin, S. T.:  
626 Anthropogenic influences on the physical state of submicron particulate matter over a tropical  
627 forest, *Atmos. Chem. Phys.*, 17, 1759–1773, doi:10.5194/acp-17-1759-2017, 2017.
- 628 Bazzaz, F. A.: Tropical Forests in a Future Climate: Changes in Biological Diversity and Impact  
629 on the Global Carbon Cycle, *Climatic Change*, 39, 317-336, doi:10.1023/A:1005359605003,  
630 1998.
- 631 Buseck, P. R. and Pósfai, M.: Airborne minerals and related aerosol particles: Effects on climate  
632 and the environment, *Proc. Natl. Acad. Sci. U.S.A.* 96, 3372-3379,  
633 doi:10.1073/pnas.96.7.3372, 1999.
- 634 Chen, Y., Shah, N., Huggins, F. E., and Huffman, G. P.: Characterization of ambient airborne  
635 particles by energy-filtered transmission electron microscopy, *Aerosol Sci. Technol.*, 39, 509–  
636 518, doi:10.1080/027868291001402, 2005.
- 637 Chen, Y., Shah, N., Huggins, F.E., and Huffman, G.P.: Microanalysis of ambient particles from  
638 Lexington, KY, by electron microscopy, *Atmos. Environ.*, 40, 651–663,  
639 doi:10.1016/j.atmosenv.2005.09.036, 2006.
- 640 Chen, H. H., Navea, J. G., Young, M. A., and Grassian, V. H.: Heterogeneous Photochemistry of  
641 Trace Atmospheric Gases with Components of Mineral Dust Aerosol, *J. Phys. Chem. A*, 115,  
642 490-499, doi:10.1021/jp110164j, 2011.
- 643 Chen, Q., Farmer, D. K., Rizzo, L. V., Pauliquevis, T., Kuwata, M., Karl, T. G., Guenther, A., Allan,  
644 J. D., Coe, H., Andreae, M. O., Pöschl, U., Jimenez, J. L., Artaxo, P., and Martin, S. T.:  
645 Submicron particle mass concentrations and sources in the Amazonian wet season (AMAZE-



- 646 08), Atmos. Chem. Phys., 15, 3687–3701, doi:10.5194/acp-15-3687-2015, 2015.
- 647 China, S., Wang, B., Weis, J., Rizzo, L., Brito, J., Cirino, G. G., Kovarik, L., Artaxo, P., Gilles, M.  
648 K., Laskin, A.: Rupturing of Biological Spores As a Source of Secondary Particles in  
649 Amazonia, Environ. Sci. Technol., 50, 12179-12186, doi: 10.1021/acs.est.6b02896, 2016.
- 650 de Sá, S. S., Palm, B. B., Campuzano-Jost, P., Day, D. A., Hu, W., Isaacman-VanWertz, G., Yee, L.  
651 D., Brito, J., Carbone, S., Ribeiro, I. O., Cirino, G. G., Liu, Y. J., Thalman, R., Sedlacek, A.,  
652 Funk, A., Schumacher, C., Shilling, J. E., Schneider, J., Artaxo, P., Goldstein, A. H., Souza, R.  
653 A. F., Wang, J., McKinney, K. A., Barbosa, H., Alexander, M. L., Jimenez, J. L., and Martin,  
654 S. T.: Urban influence on the concentration and composition of submicron particulate matter  
655 in central Amazonia, Atmos. Chem. Phys. Disc., 1-56, doi:10.5194/acp-2018-172, 2018.
- 656 Eom, H.-J., Gupta, D., Li, X., Jung, H.-J., Kim, H., and Ro, C.-U.: Influence of Collecting  
657 Substrates on the Characterization of Hygroscopic Properties of Inorganic Aerosol Particles,  
658 Anal. Chem., 86, 2648–2656, doi:10.1021/ac4042075, 2014.
- 659 Eom, H.-J., Gupta, D., Cho, H.-R., Hwang, H. J., Hur, S. D., Gim, Y., and Ro, C.-U.: Single-  
660 particle investigation of summertime and wintertime Antarctic sea spray aerosols using low-  
661 Z particle EPMA, Raman microspectrometry, and ATR-FTIR imaging techniques, Atmos.  
662 Chem. Phys., 16, 13823-13836, 10.5194/acp-16-13823-2016, 2016.
- 663 Fan, J., Rosenfeld, D., Zhang, Y., Giangran, S. E., Li, Z., Machado, L. A. T., Martin, S. T., Yang,  
664 Y., Wang, J., Artaxo, P., Barbosa, H. M. J., Braga, R. C., Comstock, J. M., Feng, Z., Gao, W.,  
665 Gomes, H. B., Mei, F., Pöhlker, C., Pöhlker, M. L., Pöschl, U., and de Souza, R. A. F.:  
666 Substantial convection and precipitation enhancements by ultrafine aerosol particles, Science,  
667 359, 411-418, 2018.
- 668 Fraund, M., Pham, D. Q., Bonanno, D., Harder, T. H., Wang, B., Brito, J., Sá, S. S. de, Carbone,  
669 S., China, S., Artaxo, P., Martin, S. T., Pöhlker, C., Andreae, M. O., Laskin, A., Gilles, M., K.,  
670 and Moffet, R. C.: Elemental Mixing State of Aerosol Particles Collected in Central  
671 Amazonia during GoAmazon2014/15, Atmosphere, 8, 173, doi:10.3390/atmos8090173, 2017.
- 672 Fung, K. H. and Tang, I. N.: Raman spectra of singly suspended supersaturated ammonium  
673 bisulfate droplets, Chem. Phys. Lett., 147, 509-513, doi:10.1016/0009-2614(88)85017-6,  
674 1988.
- 675 Fuzzi, S., Decesari, S., Facchini, M. C., Cavalli, F., Emblico, L., Mircea, M., Andreae, M. O., Trebs,  
676 I., Hoffer, A., Guyon, P., Artaxo, P., Rizzo, L. V., Lara, L. L., Pauliquevis, T., Maenhaut, W.,



- 677 Raes, N., Chi, X., Mayol-Bracero, O. L., Soto-García, L. L., Claeys, M., Kourtchev, I., Rissler,  
678 J., Swietlicki, E., Tagliavini, E., Schkolnik, G., Falkovich, A. H., Rudich, Y., Fisch, G., and  
679 Gatti, L. V.: Overview of the inorganic and organic composition of size-segregated aerosol in  
680 Rondonia, Brazil, from the biomass-burning period to the onset of the wet season, *J. Geophys.*  
681 *Res.* 112, D01201, doi:10.1029/2005JD006741, 2007.
- 682 Geng, H., Jung, H.-J., Park, Y., Hwang, H., Kim, H., Kim, Y.J., Sunwoo, Y., and Ro, C.-U.:  
683 Morphological and chemical composition characteristics of summertime atmospheric  
684 particles collected at Tokchok Island, Korea, *Atmos. Environ.* 43, 3364–3373,  
685 doi:10.1016/j.atmosenv.2009.03.034, 2009.
- 686 Geng, H., Kang, S., Choel, M., Kim, H., and Ro, C.-U.: Characterization of individual  
687 submicrometer aerosol particles collected in Incheon, Korea, by quantitative transmission  
688 electron microscopy energy-dispersive X-ray spectrometry, *J. Geophys. Res.*, 115, D15306,  
689 doi:10.1029/2009JD013486, 2010.
- 690 Geng, H., Ryu, J., Maskey, S., Jung, H.-J., and Ro, C.-U.: Characterisation of individual aerosol  
691 particles collected during a haze episode in Incheon, Korea using the quantitative ED-EPMA  
692 technique, *Atmos. Chem. Phys.* 11, 1327–1337, doi:10.5194/acp-11-1327-2011, 2011.
- 693 Geng, H., Hwang, H., Liu, X., Dong, S., and Ro, C.-U.: Investigation of aged aerosols in size  
694 resolved Asian dust storm particles transported from Beijing, China, to Incheon, Korea, using  
695 low-Z particle EPMA, *Atmos. Chem. Phys.*, 14, 3307–3323, doi:10.5194/acp-14-3307-2014,  
696 2014.
- 697 Geng, H., Jin, C.-S., Zhang, D.-P., Wang, S.-R., Xu, X.-T., Wang, X.-R., Zhang, Y, Wu, L., and Ro,  
698 C.-U.: Characterization of size-resolved urban haze particles collected in summer and winter  
699 at Taiyuan City, China using quantitative electron probe X-ray microanalysis, *Atmos. Res.*,  
700 190, 29-42, doi: 10.1016/j.atmosres.2017.02.005, 2017.
- 701 Gilardoni, S., Vignati, E., Marmer, E., Cavalli, F., Belis, C., Gianelle, V., Loureiro, A., and Artaxo,  
702 P.: Sources of carbonaceous aerosol in the Amazon basin, *Atmos. Chem. Phys.*, 11, 2747-  
703 2764, doi:10.5194/acp-11-2747-2011, 2011.
- 704 Goldstein, J., Newbury, D., Joy, D., Lyman, C., Echlin, P., Lifshin, E., Sawyer, L., and Michael, J.:  
705 Scanning Electron Microscopy and X-ray Microanalysis, third ed., Kluwer Academic/Plenum  
706 Publishers, New York, 2003.
- 707 Gregory, G. L., Harriss, R. C., Talbot, R. W., Rasmussen, R. A., Garstang, M., Andreae, M. O.,



- 708 Hinton, R. R., Browell, E. V., Beck, S. M., Sebacher, D. I., Khalil, M. A. K., Ferek, R. J., and  
709 Harriss, S. V.: Air chemistry over the tropical forest of Guyana: *J. Geophys. Res.*, 91, 8603-  
710 8612, 1986.
- 711 Haga, D. I., Burrows, S. M., Iannone, R., Wheeler, M. J., Mason, R. H., Chen, J., Polishchuk, E.  
712 A., Pöschl, U., and Bertram, A. K.: Ice nucleation by fungal spores from the classes  
713 *Agaricomycetes*, *Ustilaginomycetes*, and *Eurotiomycetes*, and the effect on the atmospheric  
714 transport of these spores, *Atmos. Chem. Phys.*, 14, 8611-8630, doi:10.5194/acp-14-8611-  
715 2014, 2014.
- 716 Hallquist, M., Wenger, J. C., Baltensperger, U., Rudich, Y., Simpson, D., Claeys, M., Dommen, J.,  
717 Donahue, N. M., George, C., Goldstein, A. H., Hamilton, J. F., Herrmann, H., Hoffmann, T.,  
718 Iinuma, Y., Jang, M., Jenkin, M. E., Jimenez, J. L., Kiendler-Scharr, A., Maenhaut, W.,  
719 McFiggans, G., Mentel, Th. F., Monod, A., Prévôt, A. S. H., Seinfeld, J. H., Surratt, J. D.,  
720 Szmigielski, R., and Wildt, J.: The formation, properties and impact of secondary organic  
721 aerosol: current and emerging issues, *Atmos. Chem. Phys.*, 9, 5155–5236, doi:10.5194/acp-  
722 9-5155-2009, 2009.
- 723 Hansen, K., Pryor, S. C., Boegh, E., Hornsby, K. E., Jensen, B., and Sørensen, L. L.: Background  
724 concentrations and fluxes of atmospheric ammonia over a deciduous forest, *Agric. For.*  
725 *Meteorol.*, 214-215, 380-392, doi:10.1016/j.agrformet.2015.09.004, 2015.
- 726 Hansen, K., Personne, E., Skjøth, C. A., Loubet, B., Ibrom, A., Jensen, R., Sørensen, L. L., and  
727 Boegh, E.: Investigating sources of measured forest-atmosphere ammonia fluxes using two-  
728 layer bi-directional modelling, *Agric. For. Meteorol.*, 237-238, 80-94,  
729 doi:10.1016/j.agrformet.2017.02.008, 2017.
- 730 Huang, P. F. and Turpin, B.: Reduction of sampling and analytical errors for electron microscopic  
731 analysis of atmospheric aerosols, *Atmos. Environ.*, 30, 4137-4148, 1996.
- 732 IBGE: Estimates of the resident population in Brazil and Federative Units, Brazilian Institute of  
733 Geography and Statistics, 2017.
- 734 Jardine, K., Yañez-Serrano, A. M., Williams, J., Kunert, N., Jardine, A., Taylor, T., Abrell, L.,  
735 Artaxo, P., Guenther, A., Hewitt, C. N., House, E., Florentino, A. P., Manzi, A., Higuchi, N.,  
736 Kesselmeir, J., Behrendt, T., Veres, P. R., Derstroff, B., Fuentes, J. D., Martin, S. T., Andreae,  
737 M. O.: Dimethyl sulfide in the Amazon rain forest, *Global Biogeochem. Cycles*, 29, 19–32,  
738 doi:10.1002/2014GB004969, 2015.





- 739 Jimenez, J. L., Canagaratna, M. R., Donahue, N. M., Prevot, A. S. H., Zhang, Q., Kroll, J. H.,  
740 DeCarlo, P. F., Allan, J. D., Coe, H., Ng, N. L., Aiken, A. C., Docherty, K. S., Ulbrich, I. M.,  
741 Grieshop, A. P., Robinson, A. L., Duplissy, J., Smith, J. D., Wilson, K. R., Lanz, V. A., Hueglin,  
742 C., Sun, Y. L., Tian, J., Laaksonen, A., Raatikainen, T., Rautiainen, J., Vaattovaara, P., Ehn,  
743 M., Kulmala, M., Tomlinson, J. M., Collins, D. R., Cubison, M. J., Dunlea, E. J., Huffman, J.  
744 A., Onasch, T. B., Alfarra, M. R., Williams, P. I., Bower, K., Kondo, Y., Schneider, J.,  
745 Drewnick, F., Borrmann, S., Weimer, S., Demerjian, K., Salcedo, D., Cottrell, L., Griffin, R.,  
746 Takami, A., Miyoshi, T., Hatakeyama, S., Shimono, A., Sun, J. Y., Zhang, Y. M., Dzepina, K.,  
747 Kimmel, J. R., Sueper, D., Jayne, J. T., Herndon, S. C., Trimborn, A. M., Williams, L. R.,  
748 Wood, E. C., Middlebrook, A. M., Kolb, C. E., Baltensperger, U., and Worsnop, D. R.:  
749 Evolution of organic aerosols in the atmosphere, *Science*, 326, 1525–1529,  
750 doi:10.1126/science.1180353, 2009.
- 751 Jordan, C., Caskey, W., Escalante, G., Herrera, R., Montagnini, F., Todd, R., and Uhl, C.: The  
752 nitrogen cycle in a ‘Terra Firme’ rainforest on oxisol in the Amazon territory of Venezuela,  
753 *Plant and Soil*, 67, 325–332, doi:10.1007/BF02182779, 1982.
- 754 Kellerhals, T., Brüttsch, S., Sigl, M., Knüsel, S., Gäggeler, H. W., and Schwikowski, M.:  
755 Ammonium concentration in ice cores: A new proxy for regional temperature reconstruction?,  
756 *J. Geophys. Res.*, 115, D16123, doi:10.1029/2009JD012603, 2010.
- 757 Kim, J. and Rees, D. C.: Nitrogenase and biological nitrogen fixation, *Biochemistry*, 33, 389–397,  
758 1994.
- 759 Krejci, R., Ström, J., Reus, M. de, Sahle, W.: Single particle analysis of the accumulation mode  
760 aerosol over the northeast Amazonian tropical rain forest, Surinam, South America, *Atmos.*  
761 *Chem. Phys.*, 5, 3331–3344, 2005.
- 762 Laskin, A., Gaspar, D. J., Wang, W., Hunt, S. W., Cowin, J. P., Colson, S. D., and Finlayson- Pitts,  
763 B. J.: Reactions at Interfaces as a Source of Sulfate Formation in Sea-Salt Particles, *Science*,  
764 301, 340–344, doi:10.1126/science.1085374, 2003.
- 765 Lei, T., Zuend, A., Cheng, Y., Su, H., Wang, W., and Ge, M.: Hygroscopicity of organic surrogate  
766 compounds from biomass burning and their effect on the efflorescence of ammonium sulfate  
767 in mixed aerosol particles, *Atmos. Chem. Phys.*, 18, 1045–1064, doi:10.5194/acp-18-1045-  
768 2018, 2018.
- 769 Lin, G., Sillman, S., Penner, J. E., and Ito, A.: Global modeling of SOA: the use of different



- 770 mechanisms for aqueous-phase formation, *Atmos. Chem. Phys.*, 14, 5451–5475,  
771 doi:10.5194/acp-14-5451-2014, 2014.
- 772 Ling, T. Y., and Chan, C. K.: Formation and transformation of metastable double salts from the  
773 crystallization of mixed ammonium nitrate and ammonium sulfate particles, *Environ. Sci. &*  
774 *Techno*, 41, 8077-8083, 10.1021/es071419t, 2007.
- 775 Mabrouk, K. B., Kauffmann, T. H., Aroui, H., and Fontana, M. D.: Raman study of cation effect  
776 on sulfate vibration modes in solid state and in aqueous solutions, *J. Raman Spectrosc*, 44,  
777 1603–1608, doi: 10.1002/jrs.4374, 2013.
- 778 Mace, K. A., Artaxo, P., and Duce, R. A.: Water-soluble organic nitrogen in Amazon Basin aerosols  
779 during the dry (biomass burning) and wet seasons, *J. Geophys. Res.*, 108(D16), 4512,  
780 doi:10.1029/2003JD003557, 2003.
- 781 Manktelow, P. T., Carslaw, K. S., Mann, G. W., and Spracklen, D. V.: The impact of dust on sulfate  
782 aerosol, CN and CCN during an East Asian dust storm, *Atmos. Chem. Phys.*, 10, 365–382,  
783 doi:10.5194/acp-10-365-2010, 2010.
- 784 Martin, S. T., Andreae, M. O., Artaxo, P., Baumgardner, D., Chen, Q., Goldstein, A. H., Guenther,  
785 A., Heald, C. L., Mayol-Bracero, O. L., McMurry, P. H., Pauliquevis, T., Pöschl, U., Prather,  
786 K. A., Roberts, G. C., Saleska, S. R., Dias, M. A. S., Spracklen, D. V., Swietlicki, E., and  
787 Trebs, I.: Sources and properties of Amazonian aerosol particles, *Rev. Geophys.*, 48, RG2002,  
788 doi:10.1029/2008rg000280, 2010a.
- 789 Martin, S. T., Andreae, M. O., Althausen, D., Artaxo, P., Baars, H., Borrmann, S., Chen, Q., Farmer,  
790 D. K., Guenther, A., Gunthe, S. S., Jimenez, J. L., Karl, T., Longo, K., Manzi, A., Müller, T.,  
791 Pauliquevis, T., Petters, M. D., Prenni, A. J., Pöschl, U., Rizzo, L. V., Schneider, J., Smith, J.  
792 N., Swietlicki, E., Tota, J., Wang, J., Wiedensohler, A., and Zorn, S. R.: An overview of the  
793 Amazonian Aerosol Characterization Experiment 2008 (AMAZE-08), *Atmos. Chem. Phys.*,  
794 10, 11415–11438, doi:10.5194/acp-10-11415-2010, 2010b.
- 795 Martin, S. T., Artaxo, P., Machado, L. A. T., Manzi, A. O., Souza, R. A. F., Schumacher, C., Wang,  
796 J., Andreae, M. O., Barbosa, H. M. J., Fan, J., Fisch, G., Goldstein, A. H., Guenther, A.,  
797 Jimenez, J. L., Pöschl, U., Silva Dias, M. A., Smith, J. N., and Wendisch, M.: Introduction:  
798 Observations and Modeling of the Green Ocean Amazon (GoAmazon2014/5), *Atmos. Chem.*  
799 *Phys.*, 16, 4785-4797, doi:10.5194/acp-16-4785-2016, 2016.
- 800 Maskey, S., Choël, M., Kang, S., Hwang, H., Kim, H., and Ro, C.-U.: The influence of collecting



- 801 substrates on the single-particle characterization of real atmospheric aerosols, *Anal. Chim.*  
802 *Acta*, 658, 120-127, doi:10.1016/j.aca.2009.11.006, 2010.
- 803 Millstein, D. E., Harley, R. A., and Hering, S. V.: Weekly cycles in fine particulate nitrate, *Atmos.*  
804 *Environ.* 42, 632–641, doi:10.1016/j.atmosenv.2007.10.010, 2008.
- 805 Möhler, O., Benz, S., Saathoff, H., Schnaiter, M., Wagner, R., Schneider, J., Walter, S., Ebert, V.,  
806 Wagner, S.: The effect of organic coating on the heterogeneous ice nucleation efficiency of  
807 mineral dust aerosols, *Environ. Res. Lett.*, 3, 025007, doi:10.1088/1748-9326/3/2/025007,  
808 2008.
- 809 Moran-Zuloaga, D., Ditas, F., Walter, D., Saturno, J., Brito, J., Carbone, S., Chi, X., de Angelis, I.  
810 H., Baars, H., Godoi, R. H. M., Heese, B., Holanda, B. A., Lavrič, J.V., Martin, S. T., Ming,  
811 J., Pöhlker, M. L., Ruckteschler, N., Su, H., Wang, Y., Wang, Q., Wang, Z., Weber, B., Wolff,  
812 S., Artaxo, P., Pöschl, U., Andreae, M. O., and Pöhlker, C.: Long-term study on coarse mode  
813 aerosols in the Amazon rain forest with the frequent intrusion of Saharan dust plumes, *Atmos.*  
814 *Chem. Phys.* 18, 10055-10088, doi.:10.5194/acp-18-10055-2018, 2018.
- 815 Neill, C., Piccolo, M. C., Melillo, J. M., Steudler, P. A., Cerri, C. C.: Nitrogen dynamics in Amazon  
816 forest and pasture soils measured by <sup>15</sup>N pool dilution, *Soil Biol. Biochem.*, 31, 567-572,  
817 1999.
- 818 Palm, B. B., de Sá, S. S., Day, D.A., Campuzano-Jost, P., Hu, W., Seco, R., Sjostedt, S. J., Park,  
819 J.-H., Guenther, A. B., Kim, S., Brito, J., Wurm, F., Artaxo, P., Thalman, R., Wang, J., Yee, L.  
820 D., Wernis, R., Isaacman-VanWertz, G., Goldstein, A. H., Liu, Y., Springston, S. R., Souza,  
821 R., Newburn, M. K., Alexander, M. L., Martin, S.T., and Jimenez, J. L.: Secondary organic  
822 aerosol formation from ambient air in an oxidation flow reactor in central Amazonia, *Atmos.*  
823 *Chem. Phys.*, 18, 467–493, doi.:10.5194/acp-18-467-2018, 2018.
- 824 Pöhlker, C., Wiedemann, K. T., Sinha, B., Shiraiwa, M., Gunthe, S. S., Smith, M., Su, H., Artaxo,  
825 P., Chen, Q., Cheng, Y. F., Elbert, W., Gilles, M. K., Kilcoyne, A. L. D., Moffet, R. C.,  
826 Weigand, M., Martin, S. T., Poeschl, U., and Andreae, M. O.: Biogenic potassium salt  
827 particles as seeds for secondary organic aerosol in the Amazon, *Science*, 337, 1075–1078,  
828 doi:10.1126/science.1223264, 2012.
- 829 Pöhlker, M. L., Ditas, F., Saturno, J., Klimach, T., Hrabě de Angelis, I., Araújo, A. C., Brito, J.,  
830 Carbone, S., Cheng, Y., Chi, X., Ditz, R., Gunthe, S. S., Holanda, B. A., Kandler, K.,  
831 Kesselmeier, J., Könemann, T., Krüger, O. O., Lavrič, J. V., Martin, S. T., Mikhailov, E.,



- 832 Moran-Zuloaga, D., Rizzo, L. V., Rose, D., Su, H., Thalman, R., Walter, D., Wang, J., Wolff,  
833 S., Barbosa, H. M. J., Artaxo, P., Andreae, M. O., Pöschl, U., and Pöhlker, C.: Long-term  
834 observations of cloud condensation nuclei over the Amazon rain forest – Part 2: Variability  
835 and characteristics of biomass burning, long-range transport, and pristine rain forest aerosols,  
836 *Atmos. Chem. Phys.*, 18, 10289–10331, doi:10.5194/acp-18-10289-2018, 2018.
- 837 Pöschl, U., Martin, S. T., Sinha, B., Chen, Q., Gunthe, S. S., Huffman, J. A., Borrmann, S., Farmer,  
838 D. K., Garland, R. M., Helas, G., Jimenez, J. L., King, S. M., Manzi, A., Mikhailov, E.,  
839 Pauliquevis, T., Petters, M. D., Prenni, A. J., Roldin, P., Rose, D., Schneider, J., Su, H., Zorn,  
840 S. R., Artaxo, P., and Andreae, M. O.: Rainforest Aerosols as Biogenic Nuclei of Clouds and  
841 Precipitation in the Amazon, *Science* 329, 1513–1516, doi:10.1126/science.1191056, 2010.
- 842 Pósfai, M., Xu, H., Anderson, and Buseck, P. R.: Wet and dry sizes of atmospheric aerosol particles:  
843 An AFM-TEM study, *Geophys. Res. Lett.* 25, 1907–1910, doi:10.1029/98GL01416, 1998.
- 844 Pósfai, M., Anderson, J. R., Buseck, P. R., and Sievering, H.: Soot and sulfate aerosol particles in  
845 the remote marine troposphere, *J. Geophys. Res.* 104, 21, 685–21, 693,  
846 doi:10.1029/1999JD900208, 1999.
- 847 Pósfai, M., Simonics, R., Li, J., Hobbs, P. V., and Buseck, P. R.: Individual aerosol particles from  
848 biomass burning in southern Africa: 1. Compositions and size distributions of carbonaceous  
849 particles, *J. Geophys. Res.*, 108(D13), 8483, doi:10.1029/2002JD002291, 2003.
- 850 Pósfai, M., Gelencser, A., Simonics, R., Arato, K., Li, J., Hobbs, P. V., and Buseck, P. R.:  
851 Atmospheric tar balls: Particles from biomass and biofuel burning, *J. Geophys. Res.*, 109,  
852 D06213, doi:10.1029/2003JD004169, 2004.
- 853 Prieto-Taboada, N., Gomez-Laserna, O., Martinez-Arkarazo, I., Olazabal, M. A., and Madariaga,  
854 J. M.: Raman Spectra of the Different Phases in the CaSO<sub>4</sub>–H<sub>2</sub>O System, *Anal. Chem.*, 86,  
855 20, 10131–10137, doi: 10.1021/ac501932f, 2014.
- 856 Qiao, T., Zhao, M., Xiu, G., and Yu, J.: Simultaneous monitoring and compositions analysis of PM<sub>1</sub>  
857 and PM<sub>2.5</sub> in Shanghai: implications for characterization of haze pollution and source  
858 apportionment, *Sci. Total Environ.*, 557–558, 386–394, doi:10.1016/j.scitotenv.2016.03.095,  
859 2016.
- 860 Rizzolo, J. A., Barbosa, C. G. G., Borillo, G. C., Godoi, A. F. L., Souza, R. A. F., Andreoli, R. V.,  
861 Manzi, A. O., Sá, M. O., Alves, E. G., Pöhlker, C., Angelis, I. H., Ditas, F., Saturno, J., Moran-  
862 Zuloaga, D., Rizzo, L. V., Rosário, N. E., Pauliquevis, T., Santos, R. M. N., Yamamoto, C. I.,



- 863 Andreae, M. O., Artaxo, P., Taylor, P. E., and Godoi, R. H. M.: Soluble iron nutrients in  
864 Saharan dust over the central Amazon rainforest, *Atmos. Chem. Phys.*, 17, 2673-2687,  
865 doi:10.5194/acp-17-2673-2017, 2017.
- 866 Sobanska, S., Hwang, H., Choël, M., Jung, H., Eom, H., Kim, H., Barbillat, J., and Ro, C.-U.:  
867 Investigation of the chemical mixing state of individual Asian Dust particles by the combined  
868 use of Electron Probe X-ray Microanalysis and Raman Microspectrometry, *Anal. Chem.*, 84,  
869 3145-3154, doi:10.1021/ac2029584, 2012.
- 870 Sullivan, R. C., Guazzotti, S. A., Sodeman, D. A., and Prather, K. A.: Direct observations of the  
871 atmospheric processing of Asian mineral dust, *Atmos. Chem. Phys.*, 7, 1213-1236,  
872 doi:10.5194/acp-7-1213-2007, 2007.
- 873 Sutton, M.A., Nemitz, E., Milford, C., Campbell, C., Erisman, J. W., Hensen, A., Cellier, P., David,  
874 M., Loubet, B., Personne, E., Schjoerring, J. K., Mattsson, M., Dorsey, J. R., Gallagher, L.,  
875 Horvath, M. W., Weidinger, T., Meszaros, R., Dämmgen, U., Neftel, A., Herrmann, B.,  
876 Lehman, B. E., Flechard, C., and Burkhardt, J.: Dynamics of ammonia exchange with cut  
877 grassland: synthesis of results and conclusions of the GRAMINAE integrated experiment.  
878 *Biogeosciences* 6, 2907–2934. doi:10.5194/bg-6-2907-2009, 2009.
- 879 Sutton, M.A., Reis, S., Riddick, S.N., Dragosits, U., Nemitz, E., Theobald, M. R., Tang, Y. S.,  
880 Braban, C. F., Vieno, M., Dore, A. J., Mitchell, R. F., Wanless, S., Daunt, F., Fowler, D.,  
881 Blackall, T. D., Milford, C., Flechard, C. R., Loubet, B., Massad, R., Cellier, P., Personne, E.,  
882 Coheur, P. F., Clarisse, L., Van Damme, M., Ngadi, Y., Clerbaux, C., Skjøth, C. A., Geels, C.,  
883 Hertel, O., Wichink Kruit, R. J., Pinder, R. W., Bash, J. O., Walker, J. T., Simpson, D., Horvath,  
884 L., Misselbrook, T. H., Bleeker, A., Dentener, F., and de Vries, W.: Towards a climate-  
885 dependent paradigm of ammonia emission and deposition, *Philos. Trans. R. Soc. Lond. Ser.*  
886 *B*, 368, doi:10.1098/rstb.2013.0166, 2013.
- 887 Swap, R., Garstang, M., Greco, S., Talbot, R., and Källberg, P.: Saharan dust in the Amazon Basin,  
888 *Tellus*, 44B, 133-149, 1992.
- 889 Talbot, R. W., Andreae, M. O., Berresheim, H., Artaxo, P., Garstang, M., Harriss, R. C., Beecher,  
890 K. M., and Li, S. M.: Aerosol chemistry during the wet season in Central Amazonia: The  
891 influence of long-range transport, *J. Geophys. Res.*, 95, 16,955-16,969, 1990.
- 892 ten Brink, H. M.: Reactive uptake of HNO<sub>3</sub> and H<sub>2</sub>SO<sub>4</sub> in sea-salt (NaCl) particles, *J. Aerosol Sci.*,  
893 29, 57-64, 10.1016/s0021-8502(97)00460-6, 1998.



- 894 Tobo, Y., Zhang, D., Matsuki, A., and Iwasaka, Y.: Asian dust parti-  
895 droplets under remote marine atmo- spheric conditions, *Proc. Natl. Acad. Sci. USA*, 96,  
896 3396–3403, 2010.
- 897 Tobo, Y., Prenni, A. J., DeMott, P. J., Huffman, J. A., McCluskey, C. S., Tian, G., Pöhlker, C.,  
898 Pöschl, U., and Kreidenweis, S. M.: Biological aerosol particles as a key determinant of ice  
899 nuclei populations in a forest ecosystem, *J. Geophys. Res.*, 118, 10100-10110,  
900 doi:10.1002/jgrd.50801, 2013.
- 901 Vekemans, B., Janssens, K., Vincze, L., Adams, F., and Van Espen, P.: Analysis of X-ray spectra  
902 by iterative least squares (AXIL): New developments, *X-Ray Spectrom.* 23, 278-285, 1994.
- 903 Wang, A., Freeman, J. J., Jolliff, B. L., and Chou I-M.: Sulfates on Mars: A systematic Raman  
904 spectroscopic study of hydration states of magnesium sulfates, *Geochim. Cosmochim.*  
905 *Acta*, 70, 611, doi:10.1016/j.gca.2006.05.022, 2006.
- 906 Wang, B., Harder, T. H., Kelly, S. T., Piens, D. S., China, S., Kovarik, L., Keiluweit, M., Arey,  
907 B. W., Gilles, M. K., and Laskin, A.: Airborne soil organic particles generated by precipitation,  
908 *Nature Geosci.* 9, 433–437, doi:10.1038/ngeo2705, 2016.
- 909 Worobiec, A., de Hoog, J., Osan, J., Szaloki, I., Ro, C.-U., and Van Grieken, R.: Thermal  
910 stability of beam sensitive atmospheric aerosol particles in electron probe microanalysis at  
911 liquid nitrogen temperature, *Spectrochim. Acta B* 58, 479–496, 2003.
- 912 Wright, S. J.: Phenological responses to seasonality in tropical forest plants, 440-460, in *Tropical*  
913 *Forest Plant Ecophysiology*, Mulkey S. S., Chazdon, R. L., and Smith A. P. (Eds), Springer,  
914 1996.
- 915 Yeung, M. C., and Chan, C. K.: Water content and phase transitions in particles of inorganic and  
916 organic species and their mixtures using Micro-Raman Spectroscopy, *Aerosol Sci. Technol.*,  
917 4, 269-280, doi:10.1080/02786820903583786, 2010.
- 918 Zhang, R., Khalizov, A. F., Khalizov, J., Zhang, D., Xue, H., and McMurry, P. H.: Variability in  
919 morphology, hygroscopicity, and optical properties of soot aerosols during atmospheric  
920 processing, *Proc. Natl. Acad. Sci. U. S. A.*, 105, 10,291–10,296,  
921 doi:10.1073/pnas.0804860105, 2008.



Figure 1. Location of sampling sites at the Brazilian Amazon basin: an urban site in Manaus (S 3°05.753' W 59°59.419') and a rainforest site at ATTO (S 02°647' W 58°59.992'). Map of South America (top left) with the region marked with a red rectangle and a map of the Amazonas state, Brazil (bottom left) also with the region of interest marked in red.

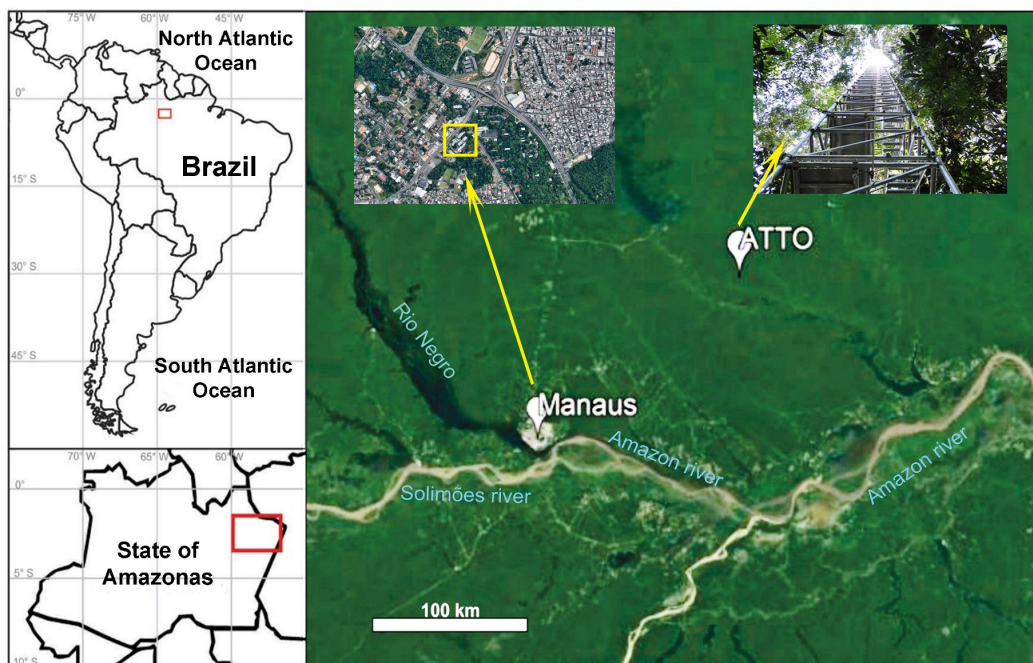
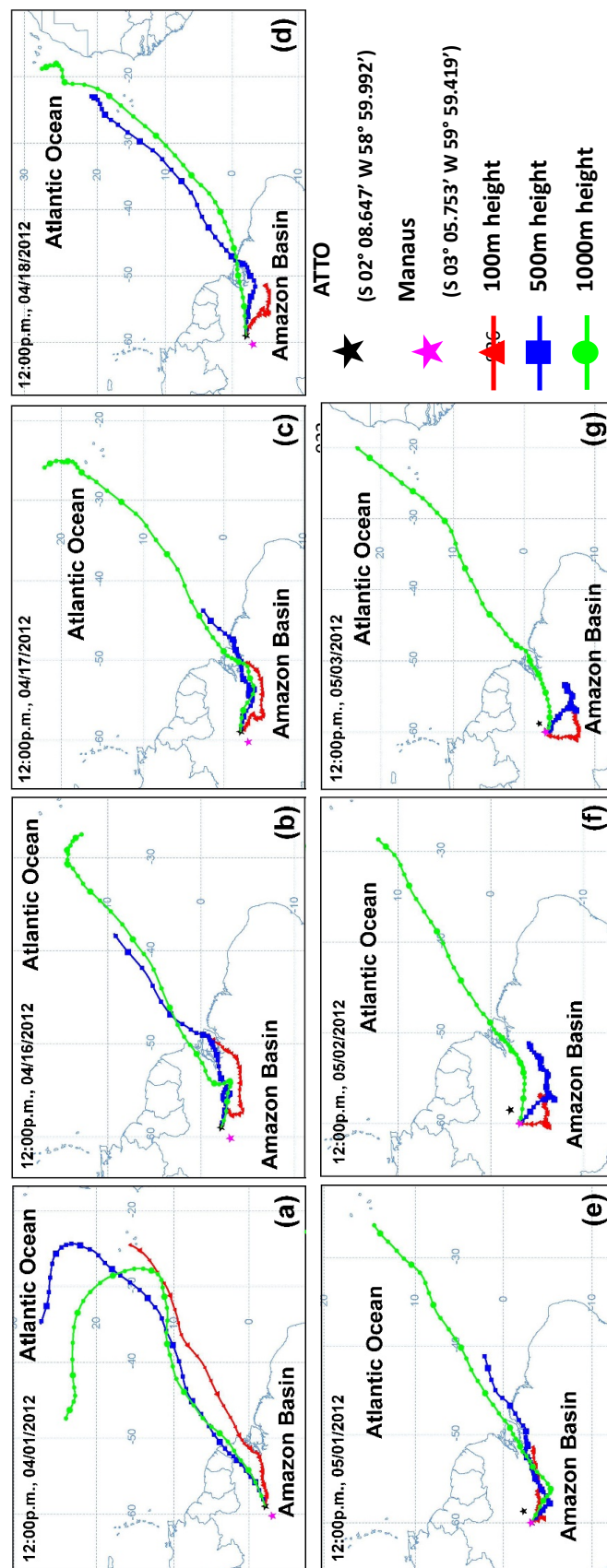




Figure 2. Ten-day (240 h) backward air mass trajectories at 100 m-, 500 m-, and 1000 m-receptor heights; (a)-(d) for the SA1-SA4 samples collected on April 1 and 16-18, 2012 at the ATTO site and (e)-(g) for the SM1-SM3 samples collected on May 1-3, 2012 at the Manaus site. HYbrid Lagrangian Single-Particle Integrated Trajectory (HYSPLIT) model available at the NOAA Air Resources Laboratory's web server (<http://www.arl.noaa.gov/ready/hysplit4.html>) was used



929





Figure 3. Home-made sample holder for TEM grid samples in SEM/EDX measurements and a typical X-ray spectrum of the TEM grids.

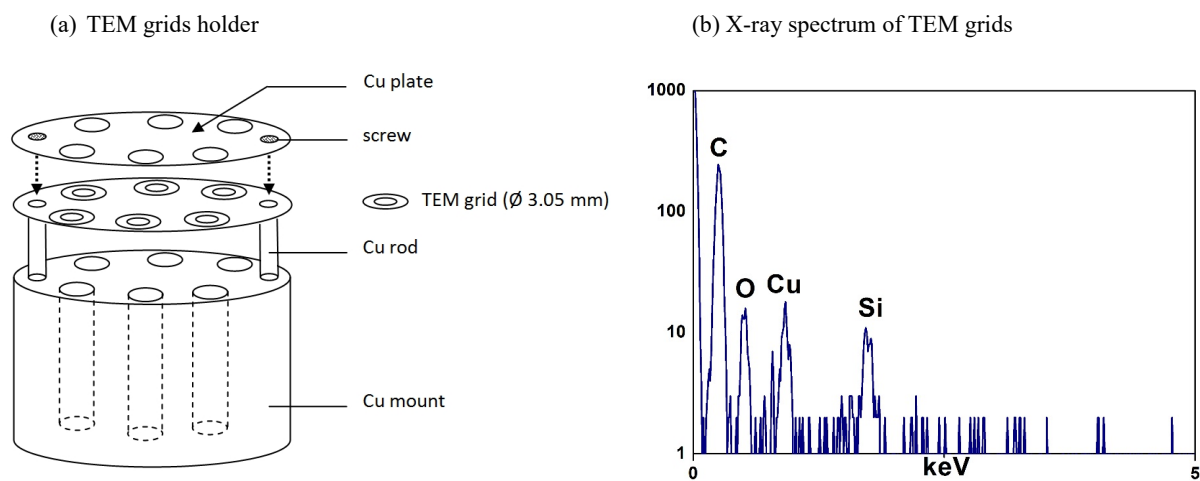






Figure 5. Typical SEM images of aerosol particles for (a) stage 1 ( $PM_{0.25-0.5}$ ) of the SM1 sample, (b) stage 2 ( $PM_{0.5-1.0}$ ) of the SM2 sample, (c) stage 3 ( $PM_{1-2}$ ) of the SM1 sample, and (d) stage 4 ( $PM_{2.0-4.0}$ ) of the SM3 sample, collected at the Manaus site. For convenience, ammonium sulfate, secondary organic aerosol, aluminosilicates, and reacted sea-salt are denoted as “AS”, “SOA”, “AlSi”, and “rss”, respectively.

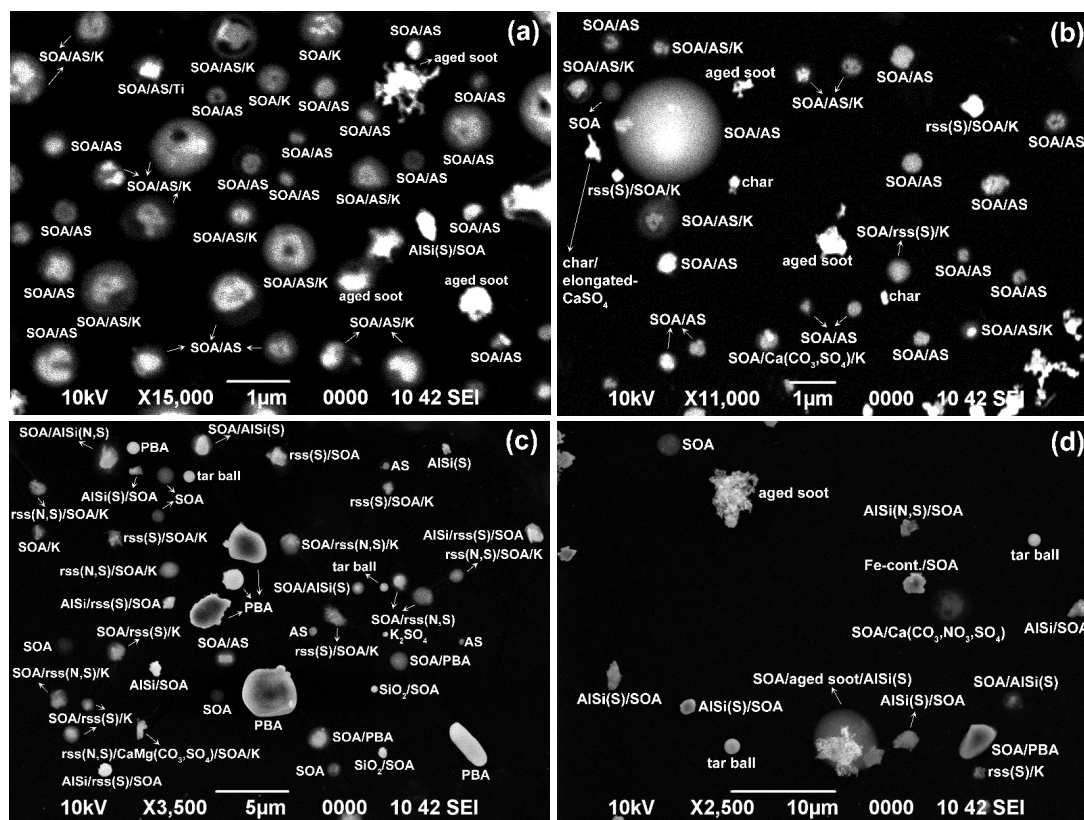




Figure 6. SEIs, X-ray spectra, and element atomic concentrations of SOA, ammonium sulfate (AS), and mixture particles. The inset images in (b), (c), and (f) show the beam damage on the particles after X-ray measurements.

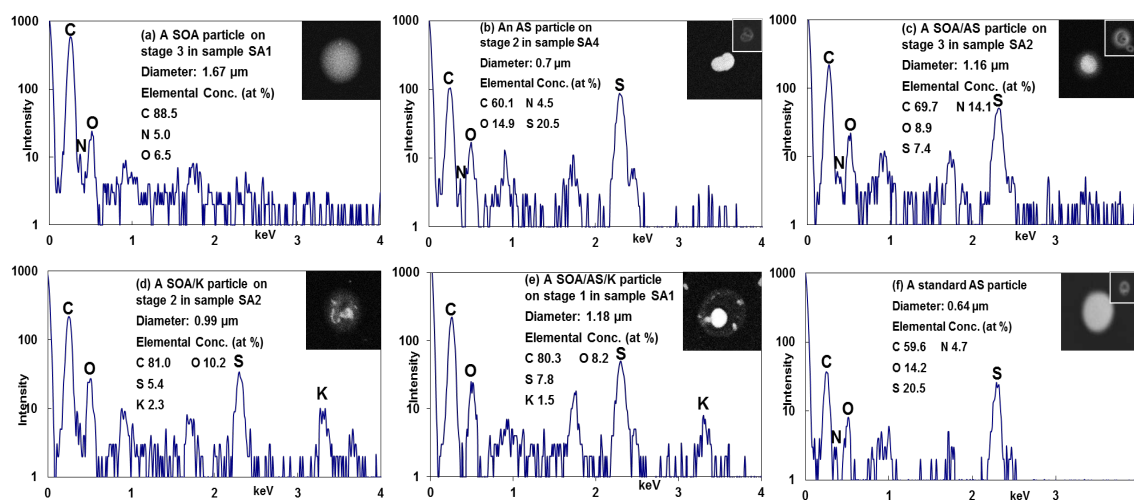




Figure 7. (a) Raman spectra of standard and airborne ammonium sulfate (AS) particles, which were rescaled for clarity. The inset SEI images are for standard and airborne AS particles where the scale bar is 1  $\mu\text{m}$ . The shoulder peak of  $\text{SO}_4^{2-}$  at  $982\text{ cm}^{-1}$  in the airborne AS particles is from  $\text{K}_2\text{SO}_4$ ; (b) SEI, optical images, X-ray, ATR-FTIR, and Raman spectra of an overloaded  $\text{PM}_{0.25-0.5}$  sample collected at ATTO site on June 10, 2014. X-ray, ATR-FTIR, and Raman spectra indicate that AS, organics, and minerals are the major components of the submicron sample. The sloping baseline in the airborne Raman spectrum is due to the fluorescence from organic compounds.

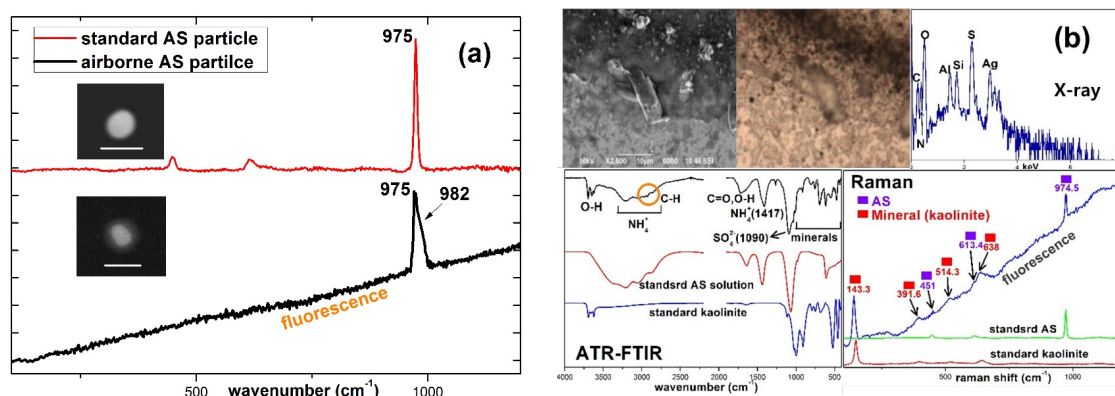




Figure 8. SEIs, X-ray spectra, and element atomic concentrations of aged mineral dust particles.

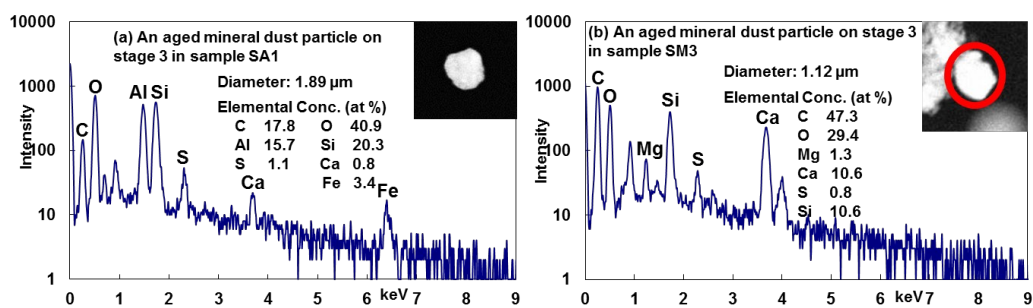




Figure 9. Number abundances of reacted sea-salt and aged mineral dust particles containing sulfates (■), nitrates (■), and both (■).

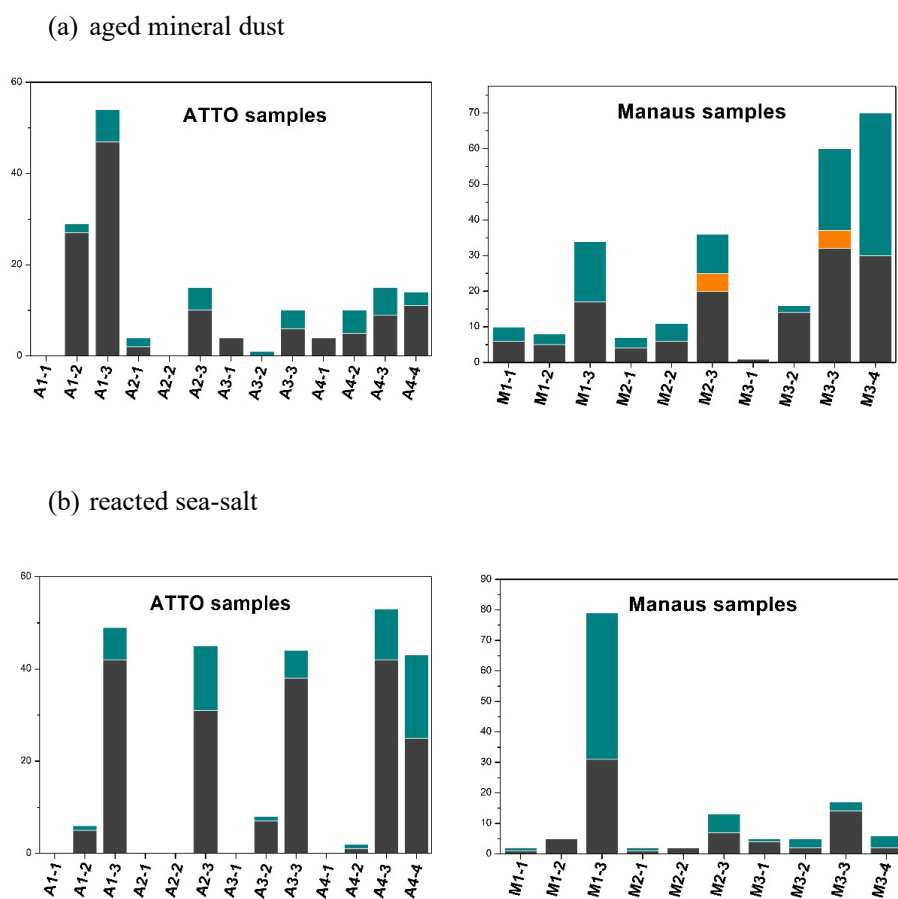




Figure 10. SEIs, X-ray spectra, and element atomic concentrations of (a) reacted sea-salt, (b) reacted sea-salt with K-salt, and (c) elongated  $\text{CaSO}_4$

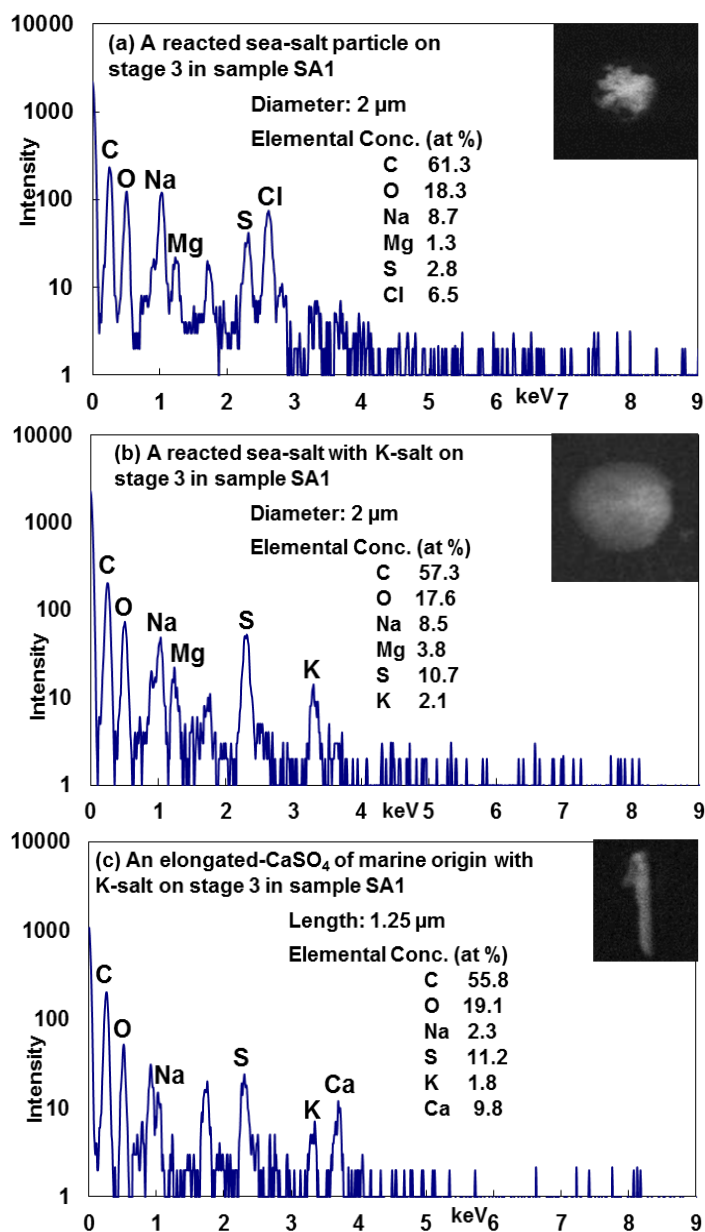






Figure 11. SEIs, X-ray spectra, and element atomic concentrations of (a) PBA, (b) soot, (c) tar call, (d) fly ash, (e) Ni-containing, and (f) Fe-containing particles.

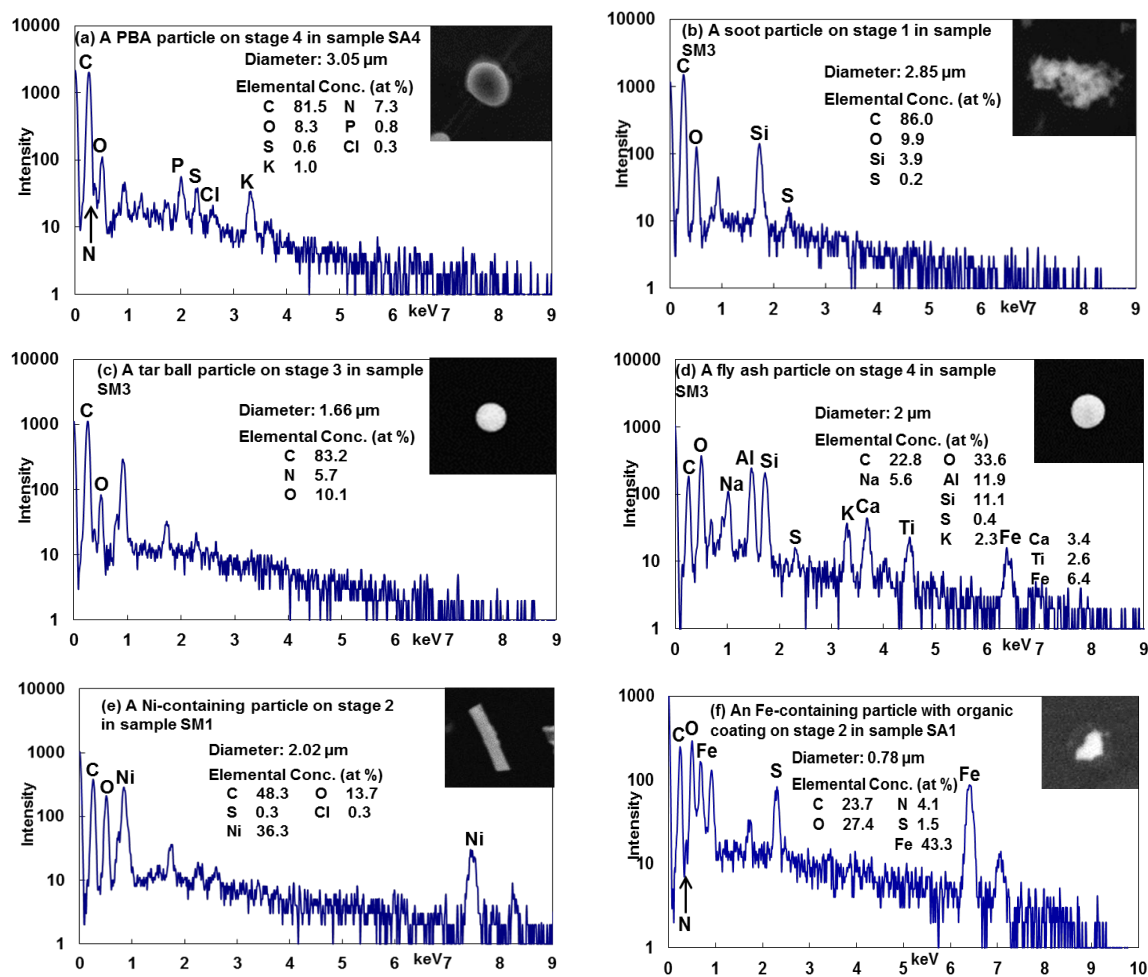




Figure 12. Typical SEIs of PBA particles from stage 4 of the (a) SA4 and (b) SM3 samples. PBA and PBA/SOA mixture particles are marked with (→) and (+), respectively.

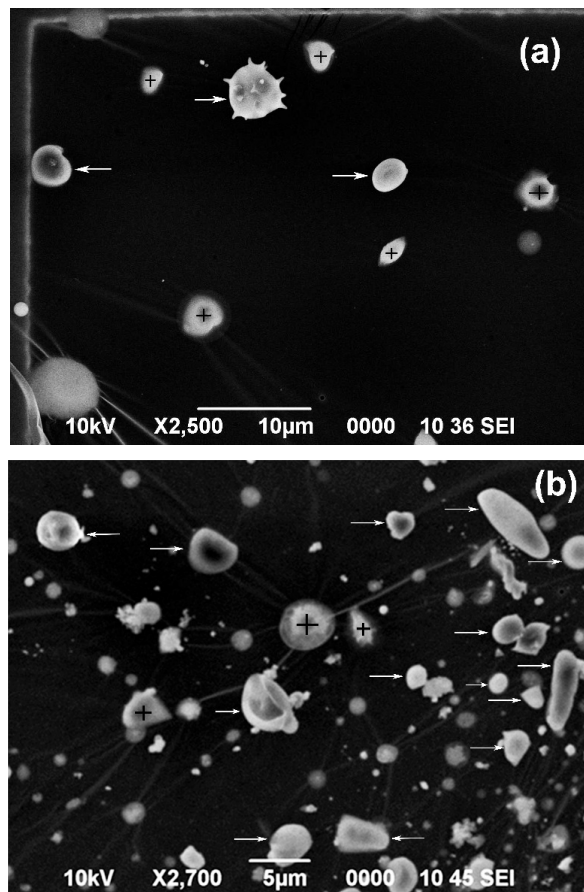




Figure 13. Relative abundance of nine different particle types for the SA1-SA4 and SM1-SM3 samples collected at the ATTO and Manaus sites, respectively.

